Available online at www.sciencedirect.com
ScienceDirect
Journal of Sound and Vibration 322 (2009) 401–437
JOURNAL OF SOUND AND VIBRATION
www.elsevier.com/locate/jsvi

Interaction between an external shock wave and a cylindrical shell filled with and submerged into different fluids

S. Iakovlev

Department of Engineering Mathematics and Internetworking, Dalhousie University, Halifax, Nova Scotia, Canada B3J 2X4

Received 6 February 2008; received in revised form 22 September 2008; accepted 6 November 2008
Handling Editor: S. Bolton
Available online 7 February 2009

Abstract

A submerged fluid-filled cylindrical shell subjected to an external shock wave is addressed for the most general case when the internal and external fluids have different properties. Three distinctly different scenarios of interaction are identified depending on the parameter ζ defined as the ratio of the acoustic speed in the internal fluid to that in the external one. The first scenario corresponds to the values of ζ below unity, and it can follow two sub-scenarios that exhibit qualitatively different focusing and reflection sequences, with the transition between the sub-scenarios occurring at $\zeta \approx 0.52$. The second scenario, $\zeta = 1$, corresponds to the relatively well-studied case of two identical fluids, yet some interesting, previously unreported effects are observed for such ζ as well. The third scenario corresponds to the values of ζ above unity, and it also exhibits a number of unique features of the wave propagation and reflection. The dynamics of the complete internal-external field is visualized and analyzed for the three scenarios, with the emphasis on both the theoretical significance of the effects observed and their practical implications.

1. Introduction

When one is concerned with the analysis of the shock response of a fluid-filled submerged thin-walled structure, often the scenario where the internal and external fluids have different properties is of interest. Underwater pipelines and storage tanks, cooling systems of chemical and nuclear reactors, and submersible vehicles are all examples of engineering structures that simultaneously interact with two different fluids. From the practical point of view, therefore, studying the shell-shock interaction under the assumption of different properties of the internal and external fluids appears to be of particular importance. However, to the best of the author's knowledge, this most general case does not seem to have been addressed for a cylindrical shell, at least as far as analyzing the hydrodynamic fields induced during the interaction is concerned. The present paper aims at filling this gap.

Historically, the early studies of shell-shock interaction were mostly focused on the structural aspects of the process, aiming at providing the naval architects and ocean engineers with the most critical estimates needed at the initial stages of the ship and submarine design, such as maximum stresses in and deflections of the

E-mail address: serguei.iakovlev@dal.ca

0022-460X/$ - see front matter © 2008 Elsevier Ltd. All rights reserved.
doi:10.1016/j.jsv.2008.11.037

Nomenclature

c_i	sound speed in the internal fluid, $\hat{c}_i = c_i c_e^{-1}$
c_e	sound speed in the external fluid, $\hat{c}_e = 1$
c_s	sound speed in the shell material, $\hat{c}_s = c_s c_e^{-1}$
h_0	thickness of the shell, $\hat{h}_0 = h_0 r_0^{-1}$
I_n	modified Bessel function of the first kind of order n
K_n	modified Bessel function of the second kind of order n
p_α	peak incident pressure, $\hat{p}_\alpha = p_\alpha \rho_e^{-1} c_e^{-2}$
p	total pressure in the fluid, $\hat{p} = p \rho_e^{-1} c_e^{-2}$
p_0	incident pressure, $\hat{p}_0 = p_0 \rho_e^{-1} c_e^{-2}$
p_d	diffraction pressure, $\hat{p}_d = p_d \rho_e^{-1} c_e^{-2}$
p_r^i	internal radiation pressure, $\hat{p}_r^i = p_r^i \rho_e^{-1} c_e^{-2}$
p_r^e	external radiation pressure, $\hat{p}_r^e = p_r^e \rho_e^{-1} c_e^{-2}$
r	radial coordinate of the polar coordinate system, $r = \varrho r_0^{-1}$
r_0	radius of the shell, $\hat{r}_0 = 1$
R_0	radial distance to the source of the incident wave, $\hat{R}_0 = R_0 r_0^{-1}$
S_R	incident shock wave stand-off, $\hat{S}_R = S_R r_0^{-1}$
t	time, $t = \tau c_e r_0^{-1}$
v^*	transverse displacement of the middle surface of the shell, $v = v^* r_0^{-1}$
w^*	normal displacement of the middle surface of the shell, $w = w^* r_0^{-1}$
E_s	Young's modulus, $\hat{E}_s = E_s \rho_e^{-1} c_e^{-2}$
ζ	ratio of the acoustics speeds in the internal and external fluids, $\zeta = c_i c_e^{-1}$
θ	angular coordinate of the polar coordinate system
λ	exponential decay rate, $\hat{\lambda} = \lambda c_e r_0^{-1}$
ν	Poisson's ratio
ξ_n^i	internal response functions
ξ_n^e	external response functions
ρ_i	density of the internal fluid, $\hat{\rho}_i = \rho_i \rho_e^{-1}$
ρ_e	density of the external fluid, $\rho_e = 1$
ρ_s	density of the shell material, $\hat{\rho}_s = \rho_s \rho_e^{-1}$
ϱ	radial coordinate of the polar coordinate system, $r = \varrho r_0^{-1}$
τ	time, $t = \tau c_e r_0^{-1}$
ϕ	fluid velocity potential in the fluid, $\hat{\phi} = \phi c_e^{-1} r_0^{-1}$
ϕ_i	fluid velocity potential in the internal fluid, $\hat{\phi}_i = \phi_i c_e^{-1} r_0^{-1}$
ϕ_e	fluid velocity potential in the external fluid, $\hat{\phi}_e = \phi_e c_e^{-1} r_0^{-1}$
ϕ_0	fluid velocity potential in the incident wave, $\hat{\phi}_0 = \phi_0 c_e^{-1} r_0^{-1}$
ϕ_d	fluid velocity potential in the diffracted wave, $\hat{\phi}_d = \phi_d c_e^{-1} r_0^{-1}$
ϕ_r^i	fluid velocity potential in the internal radiated wave, $\hat{\phi}_r^i = \phi_r^i c_e^{-1} r_0^{-1}$
ϕ_r^e	fluid velocity potential in the external radiated wave, $\hat{\phi}_r^e = \phi_r^e c_e^{-1} r_0^{-1}$

$(*)_n \sin n\theta$ and $(*)_n \cos n\theta$ denote the harmonics of (*). Unless stated otherwise, capitalized symbols denote the Laplace transforms of the corresponding functions. Other symbols are defined in the text.

structure's walls. The earliest work dealt with analysis of a few lowest modes and/or early-time approximations (e.g. Refs. [1,2]), and several years later the first papers where complete time-histories of the displacements and strains and/or surface pressure were analyzed were published (e.g. Refs. [3,4]), even though most still considered two-dimensional simplifications of the interaction. By the early 1970s, rather realistic three-dimensional structural analysis became possible (e.g. Refs. [5,6]), which continued to advance through the decade, within the limitations imposed by the computational technologies of the time. The vast majority of the work published in the 1950s–1970s was devoted to a submerged evacuated shell, a trend that is not surprising at all if put in the historical context.

Even though quality experimental images of the shock wave diffraction on cylinders date back to as early as the 1960s (e.g. Refs. [7,8]), the experimental studies of the interaction between elastic shells and shock waves (or non-stationary acoustic pulses) published in the 1960s and 1970s appear to be somewhat limited. An extensive and richly illustrated study of the acoustic fields in and around cylindrical shells (or rigid cylinders) submerged in and/or filled with fluid and subjected to various acoustic pulses ([9] and also Refs. [10,11])

appears to be one of the most informative investigations published up until the late 1990s in which actual images of the acoustic fields induced by a non-stationary loading on an elastic shell were shown. Even though the incident loads considered were mostly partially insonifying acoustic pulses and rays, the images presented in the papers, especially those of the different types of radiated waves, are of considerable relevance to the present study, as well as any other investigation of fluid-contacting shells where the elastic response of a structure is a concern.

With the development of numerical methods, a major shift in the modeling of shell- and structure-shock interaction occurred from analytical approaches to numerical ones sometime in the mid 1980s. An increasingly large number of numerical studies addressing various aspects of the interaction were published in the late 1980s and through the 1990s, even though it seems that the primary focus of those studies was on rigid structures, not elastic shells (e.g. Refs. [12–16]). The elastic aspects of the interaction were addressed as well — in Ref. [17], for example, an elastic cylinder subjected to an external shock wave was considered, and the structure-radiated waves were analyzed numerically; an elastic sphere was investigated experimentally in Refs. [18,19]. The study [20], where an empty submerged cylindrical shell with end closures and external stiffeners subjected to an underwater explosion was considered, and where the external hydrodynamic field and plastic deformations of the structure were simulated numerically, is an example of a numerical study addressing a structure closely approximating a real naval system.

Then, the late 1990s and the first few years of the new millennium saw an unprecedented growth in the number and sophistication of studies published on coupled interaction between shells and shock waves and/or non-stationary acoustic pulses. Ahyi, Pernod, Gatti, Latard, Merlen and Uberall [21] considered a submerged empty cylindrical shell subjected to an ultra-short acoustic pulse and presented high-quality visualizations of the corresponding acoustic field; both the scattering and radiation by the shell were addressed, with particular attention paid to the different types of the radiated waves. Sandusky, Chambers, Zerilli, Fabini and Gottwald [22] used numerical simulations to design a series of experiments aimed at detailed stress-strain analysis of a fluid-filled shell responding to an external explosion. Wardlaw and Luton [23] numerically simulated an explosion inside a fluid-filled cylindrical shell, and analyzed both a single shell and a two-shell arrangement; the influence of cavitation, a phenomenon that is often of critical importance to the adequate simulating of shock-structure interaction, was addressed as well. Chambers, Sandusky, Zerilli, Rye, Tussing and Forbes [24] studied the pressure on the inner surface of a fluid-filled shell induced by an internal explosion. Mair [25,26] complied an extensive and highly informative review of the computational approaches to the interaction between structures and underwater explosions, and discussed the existing analytical and experimental benchmarks.

As for the work pertaining specifically to shell systems incorporating two fluids, we mention the studies by Huang [27,28] who considered two concentric spherical [27] or cylindrical [28] submerged shells with fluid in between the inner and outer shells, and the investigations by Zhang and Geers [29] and Sprague and Geers [30] where a submerged filled spherical shell was addressed. Even though the solutions were obtained for the general case of different fluids in the studies mentioned, the results were presented for the case of two identical fluids (water). In the experimental study [9] mentioned earlier, a fluid-filled submerged shell was looked at in some detail as well but, again, only the case of two identical fluids was considered. Thus, it appears that the scenario where the fluids have different properties has received very little attention. Furthermore, even in the case of two identical fluids, the many shock wave propagation and reflection features of the complete internal-external hydrodynamic field, especially the more subtle secondary ones, do not seem to have been sufficiently addressed either.

In the author's earlier work [31,32], the interaction between a submerged fluid-filled cylindrical shell and a shock wave was considered in some detail as well. However, the assumption was that the same fluid is inside and outside the shell. Both wave reflection phenomena and fluid-structure interaction effects were discussed for that scenario, and it was rather obvious from the analysis of the dynamics of the process that if the fluids had been different, the wave patterns observed would have likely changed, sometimes very considerably. A preliminary investigation showed that indeed was the case, and revealed some very interesting phenomena not observed for the identical fluids. However, it was all too brief for one to render a more or less complete picture of the interaction for two different fluids. The present work offers a detailed and systematic investigation of the issue. Along with Refs. [31,32], it is also based on the author's two studies of the external field for an empty submerged shell [33,34].

2. Mathematical formulation

We consider a circular cylindrical shell of radius r_0 and thickness h_0. We assume that $h_0/r_0 \ll 1$, and that the deflections of the shell surface are small compared to its thickness, so the linear theory of thin shells can be applied. The density, Poisson's ratio, and Young's modulus of the shell material are ρ_s, ν, and E_s, respectively, and the sound speed in the shell is $c_s = E_s^{0.5}\{\rho_s(1-\nu^2)\}^{-0.5}$. The transverse and normal displacements of the middle surface of the shell are v^* and w^*, respectively. The shell is submerged into a fluid with the density ρ_e and sound speed c_e, and is filled with a fluid with the density ρ_i and sound speed c_i. Both fluids are assumed to be irrotational, inviscid, and linearly compressible.

We consider a two-dimensional simplification of the problem, i.e. assume that the incident wave has no longitudinal variation of pressure (a so-called 'cylindrical' shock wave). Although this is a very significant simplification, it still appears to be reasonable in the context of the present study: the validity, limitations, and advantages of such simplification were examined in detail in Ref. [33], and convincing arguments in favor of its use for modeling systems of the type in question were presented; the issue is further clarified here as well when the incident load is discussed. The polar coordinates (ϱ, θ) based on the axis of the shell are employed. The schematic of the problem is shown in Fig. 1.

The fluids are governed by the wave equations,

$$\nabla^2\phi_i = \frac{1}{c_i^2}\frac{\partial^2\phi_i}{\partial\tau^2} \tag{1}$$

and

$$\nabla^2\phi_e = \frac{1}{c_e^2}\frac{\partial^2\phi_e}{\partial\tau^2}, \tag{2}$$

where ϕ_i and ϕ_e are the internal and external fluid velocity potentials, respectively, and τ is time.

Under the assumption of the validity of the Love-Kirchhoff hypothesis, the shell equations in displacements are (e.g. Ref. [35]; note that here we assume the normal displacement to be positive inward, whereas in Ref. [35] it is assumed to be positive outward; as a result, some of the terms appear in the equations below with different signs than are found in that work)

$$\frac{1}{r_0^2}\frac{\partial^2 v^*}{\partial\theta^2} - \frac{1}{r_0^2}\frac{\partial w^*}{\partial\theta} + k_0^2\left(\frac{1}{r_0^2}\frac{\partial^3 w^*}{\partial\theta^3} + \frac{1}{r_0^2}\frac{\partial^2 v^*}{\partial\theta^2}\right) = \frac{1}{c_s^2}\frac{\partial^2 v^*}{\partial\tau^2}, \tag{3}$$

$$\frac{1}{r_0^2}w^* - \frac{1}{r_0^2}\frac{\partial v^*}{\partial\theta} + k_0^2\left(\frac{1}{r_0^2}\frac{\partial^4 w^*}{\partial\theta^4} + \frac{1}{r_0^2}\frac{\partial^3 v^*}{\partial\theta^3}\right) = \chi p|_{\varrho=r_0} - \frac{1}{c_s^2}\frac{\partial^2 w^*}{\partial\tau^2}, \tag{4}$$

where $k_0^2 = h_0^2/(12r_0^2)$, $\chi = (h_0\rho_s c_s^2)^{-1}$, and p is the total acoustic pressure. The pressure p is comprised several components,

$$p = p_0 + p_d + p_r^e - p_r^i, \tag{5}$$

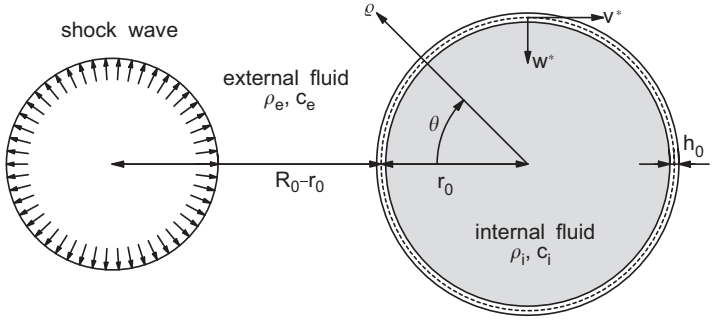

Fig. 1. Schematic of the problem.

where p_0 is the incident pressure, p_d is the diffraction pressure, p_r^i is the internal radiation pressure, and p_r^e is the external radiation pressure.

The boundary conditions of the problem include the dynamic and 'no-flow' conditions on the interface,

$$\left.\frac{\partial \phi_r^i}{\partial \varrho}\right|_{\varrho=r_0} = -\frac{\partial w^*}{\partial \tau}, \tag{6}$$

$$\left.\frac{\partial \phi_r^e}{\partial \varrho}\right|_{\varrho=r_0} = -\frac{\partial w^*}{\partial \tau}, \tag{7}$$

and

$$\left.\frac{\partial \phi_d}{\partial \varrho}\right|_{\varrho=r_0} = -\left.\frac{\partial \phi_0}{\partial \varrho}\right|_{\varrho=r_0}, \tag{8}$$

the decay conditions at the infinity

$$\phi_d \longrightarrow 0 \quad \text{and} \quad \phi_r^e \longrightarrow 0 \quad \text{when } \varrho \to \infty, \tag{9}$$

the boundedness condition on the axis of the shell,

$$-\infty < \left.\phi_r^i\right|_{\varrho=0} < \infty, \tag{10}$$

and the periodicity conditions θ-wise. The initial conditions are assumed to be zero.

The shell is subjected to an external cylindrical shock wave the pressure p_0 and potential ϕ_0 in which are given by

$$p_0 = \frac{p_\alpha S_R}{R^*} \mathrm{e}^{-(\tau - c_e^{-1}(R^* - S_R))\lambda^{-1}} \mathrm{H}(\tau - c_e^{-1}(R^* - S_R)) \tag{11}$$

and

$$\phi_0 = -\frac{\lambda p_\alpha S_R}{\rho_e R^*} \mathrm{e}^{-(\tau - c_e^{-1}(R^* - S_R))\lambda^{-1}} \mathrm{H}(\tau - c_e^{-1}(R^* - S_R)), \tag{12}$$

respectively, where

$$R^* = \sqrt{R_0^2 + \varrho^2 - 2R_0 \varrho \cos\theta}, \tag{13}$$

p_α is the pressure in the front of the wave when it first impinges on the shell, λ is the rate of exponential decay, $S_R = R_0 - r_0$ is the shock wave stand-off (the distance between the source and the shell), and H is the Heaviside unit step function.

As we mentioned earlier, some remarks need to be made regarding the wave described by Eqs. (11) and (12). Namely, the wave does not satisfy the wave equation. This fact may appear to be a very significant drawback, and one may question the validity and usefulness of a study that employs such a wave as the incident load. However, it is the author's opinion that in this particular case this is acceptable. There are two main reasons why.

First, it has been shown in Ref. [32], and further discussed in Ref. [33], that the results obtained using the *two-dimensional* wave (11) are very close to the stress-strain state observed in the middle cross-section of a the same shell subjected to a *three-dimensional* spherical shock wave, a loading scenario that is most interesting from the practical point of view. Furthermore, it was shown [36] that the middle cross-section of a shell subjected to a spherical shock wave is where the dominating stress component reaches its global maximum. Thus, using the simplified model based on Eq. (11) appears to provide the practitioner with the most critical information about the peak stresses induced by a spherical shock wave. At the same time, switching from the complete three-dimensional model to the simplified two-dimensional one dramatically reduces the respective computational time.

Second, and not less importantly, from the numerical point of view the error due to using the wave (11) instead of the actual cylindrical wave is negligibly small. Specifically, the maximum error upon substituting the

potential (12) into the two-dimensional wave equation is in the order of 5% of the equation's maximum term, and even then it is reached in very localized regions, with the rest of the fluid domain producing much lower values of the error, see Ref. [33] for details. This was further confirmed upon analyzing the images produced using the wave (12) for an empty submerged shell where it was found that the non-physical effects due to using such a wave are limited to low-magnitude negative pressure observed in the shadow zone after the incident wave passed the shell, Fig. 8 of Ref. [33]. Furthermore, the effects in question are very easy to eliminate at the post-processing stage because the pressure in the region in question is known to be zero from the physics of the shock wave diffraction. We can therefore conclude that even from the numerical point of view using the wave (11) appears to be quite acceptable.

Summarizing the above two points, we state that using the wave (11) allows one to obtain a very good approximation of the stress-strain state in the most critical region of the shell subjected to a realistic three-dimensional shock load. At the same time, the inaccuracies due to the fact that the simplified wave does not satisfy the wave equation are minimal, and are limited to low-magnitude and easy-to-eliminate non-physical pressure regions in predictable regions of the external fluid domain. The author believes that these are sufficiently solid grounds for using the wave given by (11) and (12) instead of the less complex plane one. The latter, however, is still briefly addressed later on.

We consider a dimensionless formulation of the problem, and normalize all variables to r_0, c_e, and ρ_e. Such an approach, amongst other advantages (such as the uniform applicability of the dimensionless analysis), allows for much more convenient numerical values of the time: for example, it takes two dimensionless time units for the shock wave to move over the shell, compared to several milliseconds if a dimensional formulation is considered. A hat normally distinguishes the dimensionless variables from their dimensional counterparts, with the exception of the time $t = \tau c_e r_0^{-1}$, the radial coordinate $r = \varrho r_0^{-1}$, and the normal and transverse displacements $w = w^* r_0^{-1}$ and $v = v^* r_0^{-1}$, respectively.

3. Fluid dynamics

In order to obtain the pressure components, we first apply the Laplace transform to the dimensionless wave equations (1) and (2),

$$\frac{\partial^2 \hat{\Phi}_e}{\partial r^2} + \frac{1}{r}\frac{\partial \hat{\Phi}_e}{\partial r} + \frac{1}{r^2}\frac{\partial^2 \hat{\Phi}_e}{\partial \theta^2} - s^2 \hat{\Phi}_e = 0 \tag{14}$$

and

$$\frac{\partial^2 \hat{\Phi}_i}{\partial r^2} + \frac{1}{r}\frac{\partial \hat{\Phi}_i}{\partial r} + \frac{1}{r^2}\frac{\partial^2 \hat{\Phi}_i}{\partial \theta^2} - s^2 \frac{c_e^2}{c_i^2}\hat{\Phi}_i = 0, \tag{15}$$

where $\hat{\Phi}_e$ and $\hat{\Phi}_i$ are the Laplace transforms of $\hat{\phi}_e$ and $\hat{\phi}_i$, respectively, and s is the transform variable, and then separate the spatial variables to arrive at the general solutions of Eqs. (14) and (15) in the form

$$\hat{\Phi}_e = \{F_n^e \mathrm{K}_n(rs) + G_n^e \mathrm{I}_n(rs)\}\cos n\theta, \quad n = 0, 1, \ldots \tag{16}$$

and

$$\hat{\Phi}_i = \{F_n^i \mathrm{K}_n(r\alpha s) + G_n^i \mathrm{I}_n(r\alpha s)\}\cos n\theta, \quad n = 0, 1, \ldots, \tag{17}$$

respectively, where $\alpha = c_e c_i^{-1}$, I_n is the modified Bessel function of the first kind of order n, K_n is the modified Bessel function of the second kind of order n, and F_n^e, G_n^e, F_n^i, G_n^i are arbitrary functions of s.

After the boundary conditions are imposed, the Laplace transforms of the harmonics of the three potential components are obtained,

$$\hat{\Phi}_n^d(r, \theta, s) = B_n(s)\ \Xi_n^e(r, s)\cos n\theta, \tag{18}$$

$$\hat{\Phi}_n^{r,e}(r, \theta, s) = sW_n(s)\ \Xi_n^e(r, s)\cos n\theta, \tag{19}$$

and

$$\hat{\Phi}_n^{r,i}(r,\theta,s) = -sW_n(s)\ \Xi_n^i(r,\alpha s)\cos n\theta. \tag{20}$$

Here, the expansions

$$\left.\frac{\partial\hat{\phi}_0}{\partial r}\right|_{r=1} = \sum_{n=0}^{\infty} b_n(t)\cos n\theta \tag{21}$$

and

$$w = \sum_{n=0}^{\infty} w_n(t)\cos n\theta \tag{22}$$

are assumed, W_n and B_n are the Laplace transforms of w_n and b_n, respectively, and Ξ_n^e and Ξ_n^i are the Laplace transforms of the response functions of the problem, ξ_n^e and ξ_n^i, respectively, given by

$$\Xi_n^e(r,s) = -\frac{\mathrm{K}_n(rs)}{s\mathrm{K}_n'(s)} \tag{23}$$

and

$$\Xi_n^i(r,s) = \frac{\mathrm{I}_n(rs)}{s\mathrm{I}_n'(s)}. \tag{24}$$

The expressions for the pressure harmonics can now be easily obtained,

$$\hat{p}_n^d = -\frac{1}{\sqrt{r}}b_n(t) - \int_0^t b_n(\eta)\frac{\mathrm{d}\xi_n^e}{\mathrm{d}\eta}(r,t-\eta)\,\mathrm{d}\eta, \tag{25}$$

$$\hat{p}_n^{r,e} = -\int_0^t \frac{\mathrm{d}^2 w_n(\eta)}{\mathrm{d}\eta^2}\,\xi_n^e(r,t-\eta)\,\mathrm{d}\eta, \tag{26}$$

and

$$\hat{p}_n^{r,i} = \frac{\rho_i c_i}{\rho_e c_e}\int_0^t \frac{\mathrm{d}^2 w_n(\eta)}{\mathrm{d}\eta^2}\,\xi_n^i(r,c_i c_e^{-1}(t-\eta))\,\mathrm{d}\eta, \tag{27}$$

and we arrive at the diffraction and radiation pressure in the series form,

$$p_d = \sum_{n=0}^{\infty} p_n^d\cos n\theta, \quad p_r^e = \sum_{n=0}^{\infty} p_n^{r,e}\cos n\theta, \quad \text{and} \quad p_r^i = \sum_{n=0}^{\infty} p_n^{r,i}\cos n\theta. \tag{28}$$

As is apparent from Eqs. (25)–(27), the computation of the pressure inside and outside the shell is reduced to that of the response functions.

The functions ξ_n^i and ξ_n^e represent the response of the internal and external fluids, respectively, to the motion of, or scattering by, the shell. The idea of considering the response functions as separate mathematical entities appears to have been first introduced by Geers [3], who considered a slightly different form of the 'surface' ($r = 1$) counterparts of ξ_n^e. The one-dimensional version of ξ_n^e was generalized for the case of the entire fluid domain by the author in Ref. [34] where the derivation of the analytical expressions for ξ_n^e can be found, along with the discussion of various numerical aspects, as well as that of the computational methodology employed. The internal response functions ξ_n^i were analyzed in detail in Ref. [37], where the derivation of their series expressions can be found, as well as the analysis of the series convergence and all the necessary proofs. Their applied aspect, including the physical interpretation of the functions' highly irregular nature, was addressed in Ref. [31], along with the discussion of the numerical challenges one faces when trying to compute them for the entire inner fluid domain. Even though we do not reproduce any of those results here, in order to give the reader a general idea about the response functions, and also to illustrate the fundamental difference between the physics of the response of the internal and external fluids, we include a brief discussion of ξ_n^i and ξ_n^e, as well as their graphs for several representative values of n and r.

The external response functions $\xi_n^e(r,t)$ exhibit a relatively regular behavior, Fig. 2. They have one peak value at $t = r - 1$ corresponding to the instant when the response of the shell arrives at the radial layer (r, θ). Prior to that instant, $\xi_n^e(r,t) = 0$, and after that, the functions decay as t increases, and also oscillate in a very regular way, the frequency of the oscillations increasing with n. This relatively uncomplicated behavior is representative of the quite straightforward physics of the external interaction — once generated at the shell surface, the acoustic waves propagate outward without reflecting from the shell ever again, and for every mode of the shell's motion, every point in the fluid domain is only excited once.

The internal response functions $\xi_n^i(r,t)$ exhibit a considerably less regular behavior, which is representative of the much more complex nature of the internal interaction. First of all, for every n, ξ_n^i have an infinite number of singularities and finite discontinuities, Fig. 3; the functions are shown as continuous, and the solid dots indicate the value of the functions at the points of finite discontinuity (equal to a half of the sum of the lift and right side limits at the point [37]). The finite discontinuities represent reflections of the pressure waves from the shell's interior surface, and the singularities represent the focusing of the waves at the point $r = 0$, i.e. on the axis of the shell. The singularities and finite discontinuities alternate, and their locations depend on r. In the intervals between the singularities and finite discontinuities, the functions oscillate, but do so less regularly than $\xi_n^e(r,t)$. The frequency of the oscillations increases with n, and the singularities and discontinuities approach each other when $r \to 0$. As a result, when n is large and r is small, $\xi_n^i(r,t)$ exhibit a highly irregular behavior, and are quite computationally challenging [31, Fig. 14].

From the computational point of view, the convergence of the pressure series is of importance, especially if one intends to visualize the hydrodynamic fields. The convergence of the series for the external pressure, both the diffraction and radiation one, was addressed in some detail in Ref. [34], so here we only summarize the findings of that study. The diffraction pressure was found to be the worst convergent series [34, Table 1], with as many as 300 harmonics needed to be taken into account in order to produce realistic (i.e., not exhibiting any non-physical features) two-dimensional images of pressure patterns (it was observed that a numerical error even as small as 0.5% may result in the images of the pressure patterns that have obvious non-physical features [34, Fig. 12 and Table 2]). The number of terms needed in the diffraction pressure series can be reduced to 150 if one is only concerned with reasonably accurate values of the pressure (to within 5% almost everywhere in the domain of interest) but does not intend to use the data to visualize the pressure patterns. For the external radiation pressure, 150 terms were found to be always sufficient. The series convergence for the internal pressure was addressed in Refs. [31,32], and 150 terms were observed to be sufficient for adequate

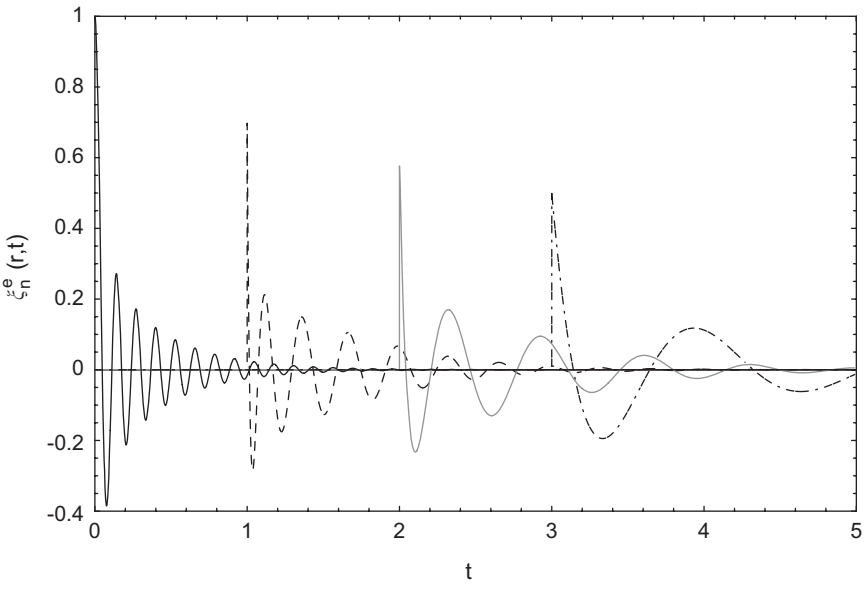

Fig. 2. External response function $\xi_n^e(r,t)$ for various r and n: $n = 50$, $r = 1.00$, solid black line; $n = 20$, $r = 2.00$, dashed black line; $n = 10$, $r = 3.00$, solid gray line; $n = 5$, $r = 4.00$, dashed-dotted black line.

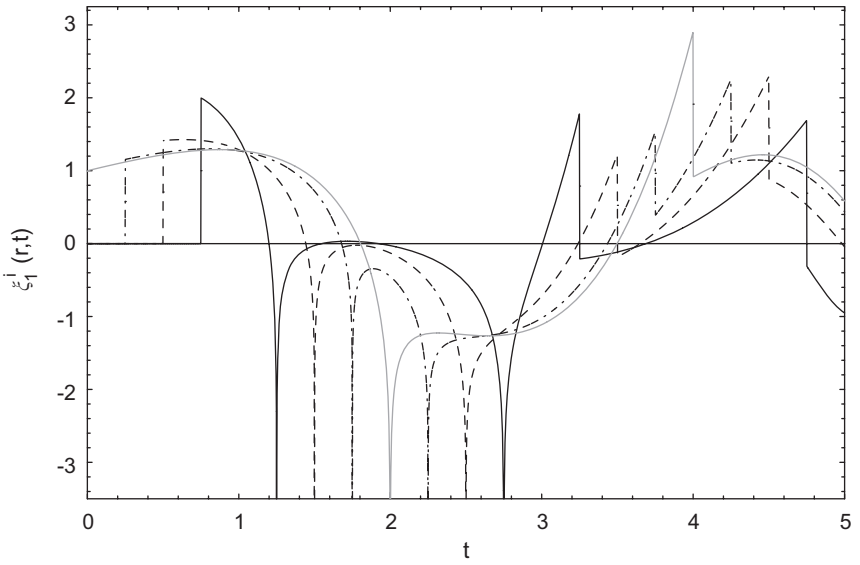

Fig. 3. Internal response function $\xi_1^i(r,t)$ for various r: $r=0.25$, solid black line; $r=0.50$, dashed black line; $r=0.75$, dashed-dotted black line; $r=1.00$, solid gray line.

visualization of the internal field. Thus, throughout the present work we always consider 150 terms in the series representing the radiation pressure (both internal and external), and 300 terms in the diffraction pressure series.

4. Structural dynamics

If we expand the displacements into the series,

$$v=\sum_{n=0}^{\infty} v_n \sin n\theta \tag{29}$$

and

$$w=\sum_{n=0}^{\infty} w_n \cos n\theta, \tag{30}$$

and rewrite the dimensionless shell equations in terms of the displacement harmonics $v_n \sin n\theta$ and $w_n \cos n\theta$, for each n we arrive at an integro-differential system for v_n and w_n,

$$\gamma^2 \frac{\mathrm{d}^2 v_n}{dt^2}+c_n^{11}v_n+c_n^{12}w_n=0, \tag{31}$$

$$\gamma^2 \frac{\mathrm{d}^2 w_n}{dt^2}+c_n^{21}v_n+c_n^{22}w_n = \hat{\chi}\left\{\hat{p}_n^0+\hat{p}_n^d-\int_0^t \frac{\mathrm{d}^2 w_n(\eta)}{\mathrm{d}\eta^2}\xi_n^e(r,t-\eta)\,\mathrm{d}\eta+\frac{\rho_i c_i}{\rho_e c_e}\int_0^t \frac{\mathrm{d}^2 w_n(\eta)}{\mathrm{d}\eta^2}\xi_n^i(r,c_i c_e^{-1}(t-\eta))\,\mathrm{d}\eta\right\}\Bigg|_{r=1}, \tag{32}$$

where

$$c_n^{11}=n^2+k_0^2 n^2,\quad c_n^{12}=c_n^{21}=-n-k_0^2 n^3,\quad c_{mn}^{22}=1+k_0^2 n^4,\quad \text{and}\quad \gamma=\hat{c}_s^{-1}. \tag{33}$$

The zero initial conditions for v_n, w_n, and their first derivatives complement Eqs. (31) and (32).

We also note that the terms in Eqs. (3) and (4) (and, consequently, Eqs. (31) and (32)) multiplied by k_0^2 represent the bending stiffness, and, generally speaking, they need to be considered to model the interaction

adequately. However, it has been demonstrated in Ref. [32], and further confirmed in Ref. [34], that for the class of fluid-structure interaction problems discussed here, neglecting the bending stiffness terms does not lead to significant changes in the acoustic field if the shell is sufficiently thin, i.e. if $h_0/r_0 \leqslant 0.01$ (the contribution of the bending stiffness terms in that case is limited to a number of very high-frequency, low-magnitude waves localized in certain, very narrow, regions). Since the focus of the present work is on the analysis of the complexity brought in by the fact that the internal and external fluids are different, of primary interest to us here are the wave phenomena in the fluids, not the relatively subtle structural dynamics features and their effect on the acoustic fields. Thus, we limit our investigation to very thin shells with the thickness-to-radius ratio of 0.01 or less, and neglect the bending stiffness.

The system (31) and (32) was approached numerically using finite differences. An explicit second-order scheme was used, with the second derivatives approximated using central differences, and the integral terms approximated using the trapezoidal rule. The scheme is admittedly simple, and one may question why a more sophisticated, higher-order scheme was not employed instead. However, since the integro-differential systems in question are ordinary, the computational time was not a determining factor here as the step size could be decreased as much as was necessary to achieve convergence. The resulting finite-difference scheme is

$$v_n^{i+1} = 2v_n^i - v_n^{i-1} - h^2\gamma^{-2}\{c_n^{11}v_n^i + c_n^{12}w_n^i\}, \tag{34}$$

$$w_n^{i+1} = 2w_n^i - w_n^{i-1} + \Omega_h\{\delta_h(p_n^i - hJ_n^i - hI_n^i) - c_n^{21}v_n^i - c_n^{22}w_n^i\}, \tag{35}$$

where $\gamma = c_e/c_s$, $\delta_h = \rho_f\gamma^2 r_0(\rho_s h_0)^{-1}$, $\Omega_h = 2h^2\rho_f\{\delta_h h(\rho_f + \rho_s\gamma^2) + 2\gamma^2\rho_f\}^{-1}$, h is the time step,

$$J_n^i = \sum_{j=1}^{i-1}\{w_n^{j+1} - 2w_n^j + w_n^{j-1}\}h^{-2}\xi_{n,ext}^{i-j} \tag{36}$$

$$I_n^i = \frac{\rho_s c_s}{\rho_f c_f}\sum_{j=1}^{i-1}\{w_n^{j+1} - 2w_n^j + w_n^{j-1}\}h^{-2}\xi_{n,int}^{i-j}, \tag{37}$$

and $\xi_{n,ext}^i$ and $\xi_{n,int}^i$ stand for the node values of $\xi_n^e(1,t)$ and $\xi_n^i(1,t)$, respectively.

The convergence of the scheme certainly is of interest and, although it has been studied in detail for the external-fluid-only problem [34], it needs to be addressed for this more complex case as well. Whether the value of ζ has any effect on the convergence is also of interest.

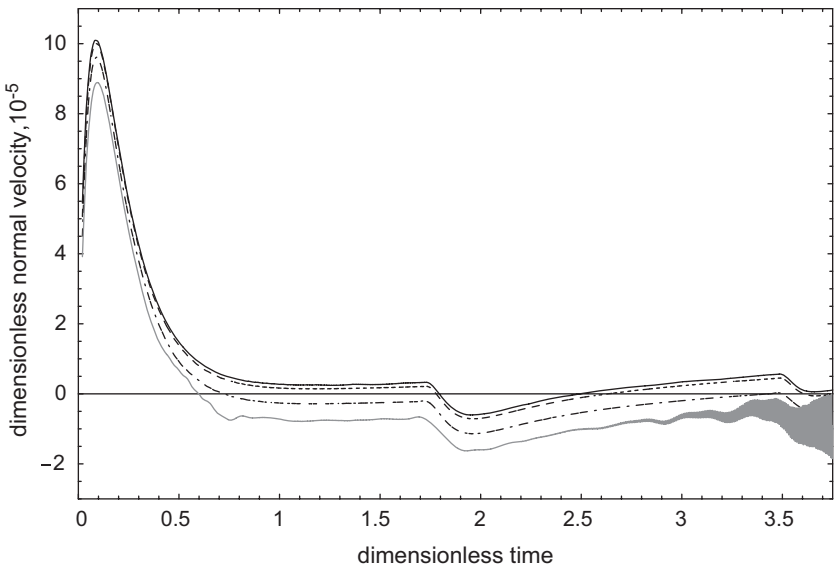

Fig. 4. Convergence of the finite-difference scheme for $\zeta = 0.50$, the bending stiffness is ignored; $h = 0.0005$, solid black line; $h = 0.001$, dashed black line; $h = 0.002$, dashed-dotted black line; $h = 0.004$, solid gray line.

Fig. 4 shows the normal velocity of the shell surface at the head point for different step sizes for $\zeta = 0.50$; the bending stiffness is ignored. One can see that when $h = 0.004$, the scheme start to diverge after $t = 2.5$. Decreasing h from 0.004 to 0.001 leads to significant changes of $\dot{w}$, but after that, the scheme appears to have converged (the average difference between $\dot{w}$ computed with $h = 0.001$ and 0.0005 is less than 2%). Thus, for this value of ζ $h = 0.001$ is sufficiently small.

When the bending stiffness is taken into account, the convergence of the scheme is noticeably worse. Although at $h = 0.0005$ the scheme still converges (and, in fact, does so even better than when the bending stiffness is ignored, with the average difference between $h = 0.001$ and 0.0005 being around 1%), it diverges much faster for larger h (the scheme becomes unstable as early as $t = 0.10$). This observation is consistent with what was seen for a submerged evacuated shell [34].

Increasing ζ results in poorer convergence, Fig. 5 ($\zeta = 1.00$). Even when the bending stiffness is ignored, the scheme becomes unstable at about $t = 0.30$ for $h = 0.004$, and at about $t = 1.50$ for $h = 0.002$. Yet, it still converges after $h = 0.001$, with the average difference between $h = 0.001$ and $h = 0.0005$ being around 2%. When the bending stiffness is taken into account, the scheme becomes unstable for $h = 0.004$ and 0.002 even before $t = 0.10$. Even then, the scheme start to converge when $h \leqslant 0.001$, and the average difference between the results produced by $h = 0.001$ and 0.0005 is in the order of 1%.

As ζ increases, the situation becomes progressively worse for all h above 0.001, both when the bending stiffness is taken into account and when it is not. However, for the entire range of ζ considered ($0.50 \leqslant \zeta \leqslant 1.50$), $h = 0.001$ has always been found to ensure convergence of the scheme and provide acceptably accurate results (the error below 5%). Thus, in our computations the step size $h = 0.001$ has been selected for all scenarios considered.

As for the convergence of the series for the strain and displacements, it has been analyzed as well. It was established that the situation here is not much different from what was seen for an empty submerged shell [34]. That is, the strain and displacement series converge much better than the pressure ones, and much fewer harmonics need to be taken into account (generally, less than 50, as opposed to 150 or even 300 required for the pressure).

5. Parameters analyzed and terminology

It was demonstrated in Ref. [32] that when the internal and external fluids are identical, the internal pressure wave is simply a geometrical continuation of the incident wave inside the shell. That, however, changes when

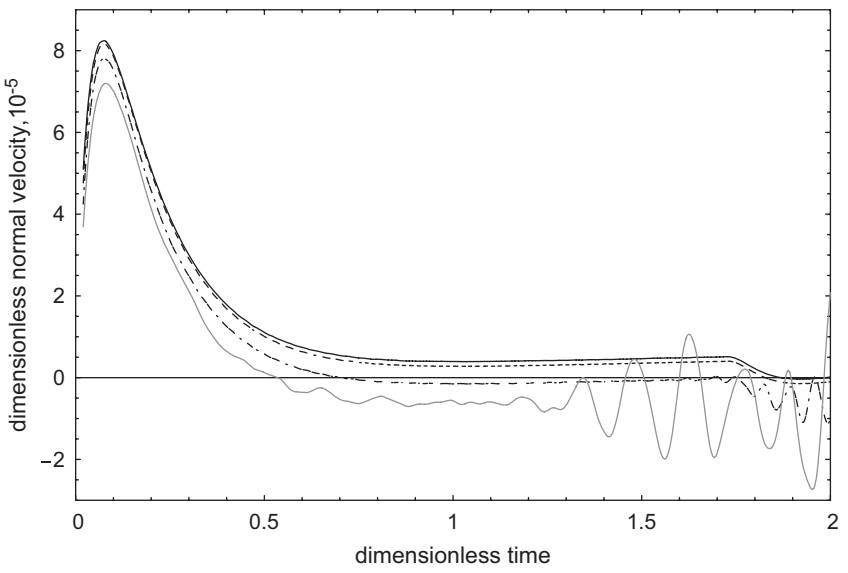

Fig. 5. Convergence of the finite-difference scheme for $\zeta = 1.00$, the bending stiffness is ignored; $h = 0.0005$, solid black line; $h = 0.001$, dashed black line; $h = 0.002$, dashed-dotted black line; $h = 0.004$, solid gray line.

the fluids are different: depending on the ratio of the acoustic speeds in the fluids, the front of the internal shock wave will be either ahead of or behind the imaginary internal continuation of the external incident wave. Since the interaction was observed to be dominated mostly by the wave reflection and focusing phenomena [31,32], such difference in the locations of the fronts will lead to significantly different wave patterns in the fluids, especially the internal one, as well as considerably different structural dynamics. The variation of the densities of the fluids will have an effect on the pressure magnitude, but not the geometry of the acoustic field. Of course, the appearance of the shell-induced component of the acoustic field also depends on the acoustic speed in the shell material. That, however, is of secondary importance due to the considerably lower magnitude of the radiated pressure.

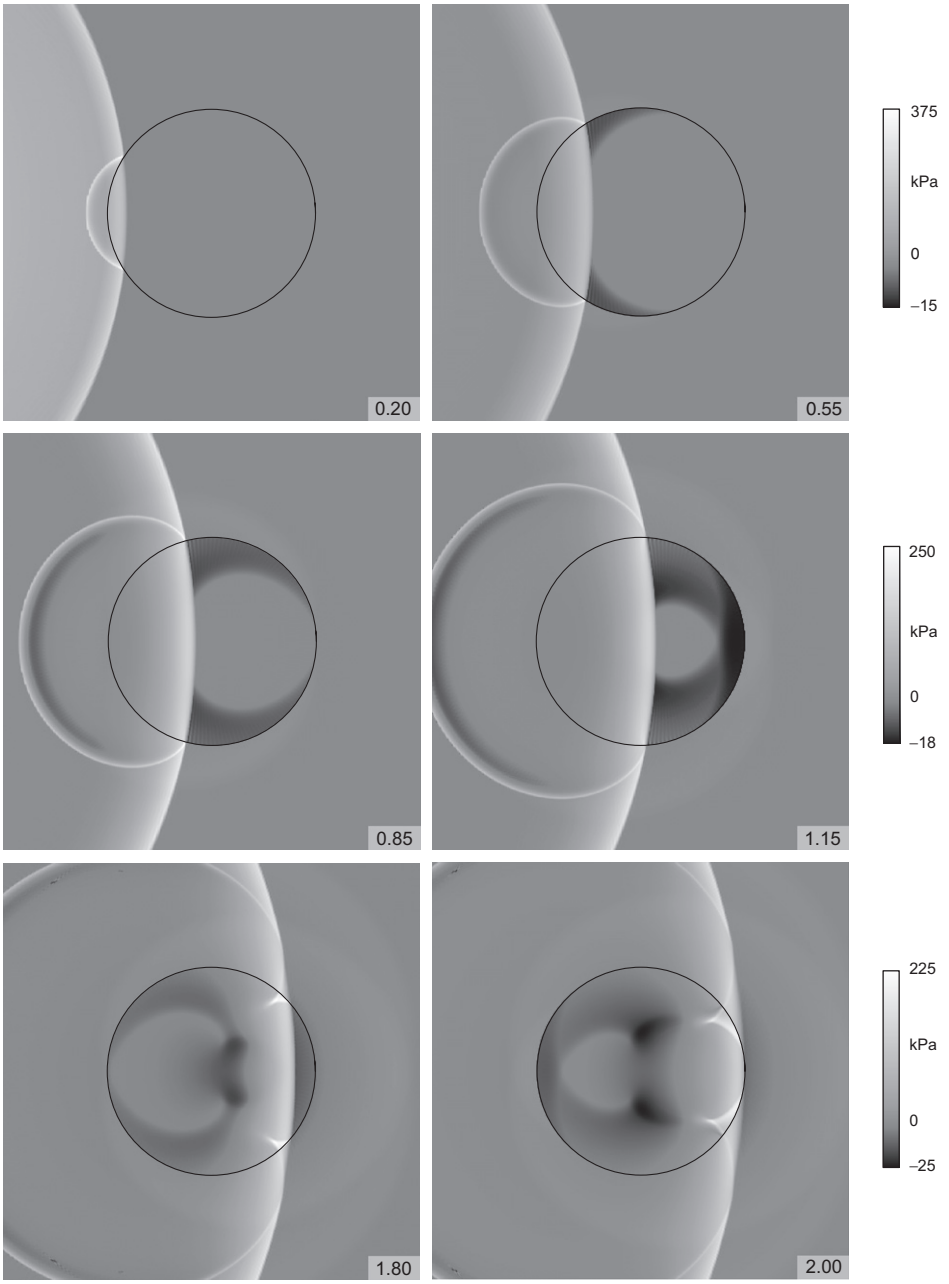

Fig. 6. Dynamics of the acoustic field in the sonic case of $\zeta = 1.00$.

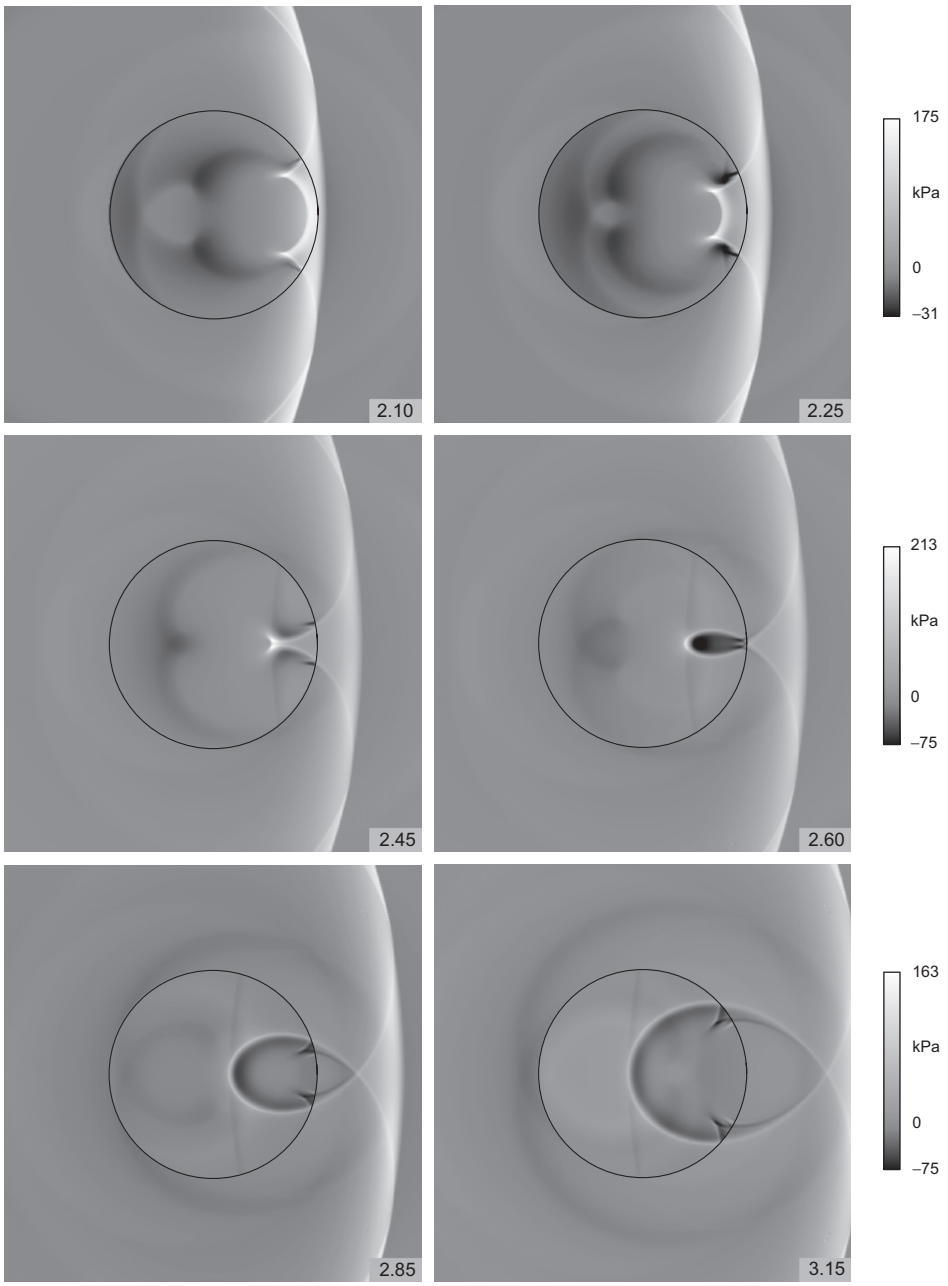

Fig. 6. (*Continued*)

It therefore appears that there is a single most important parameter that determines the appearance of the internal and external acoustic fields, namely the ratio of the acoustic speeds in the internal and external fluids. Even though this is a rather obvious conclusion, it is quite difficult to predict exactly how the acoustic fields will change when the ratio varies. Our effort, therefore, will be concentrated on determining how the change of the ratio influences the wave patterns, and, possibly, defining a few characteristic types of patterns corresponding to different ranges of the ratio. We denote this ratio of the acoustic speeds as ζ, and define it as

$$\zeta = \frac{c_i}{c_e}. \tag{38}$$

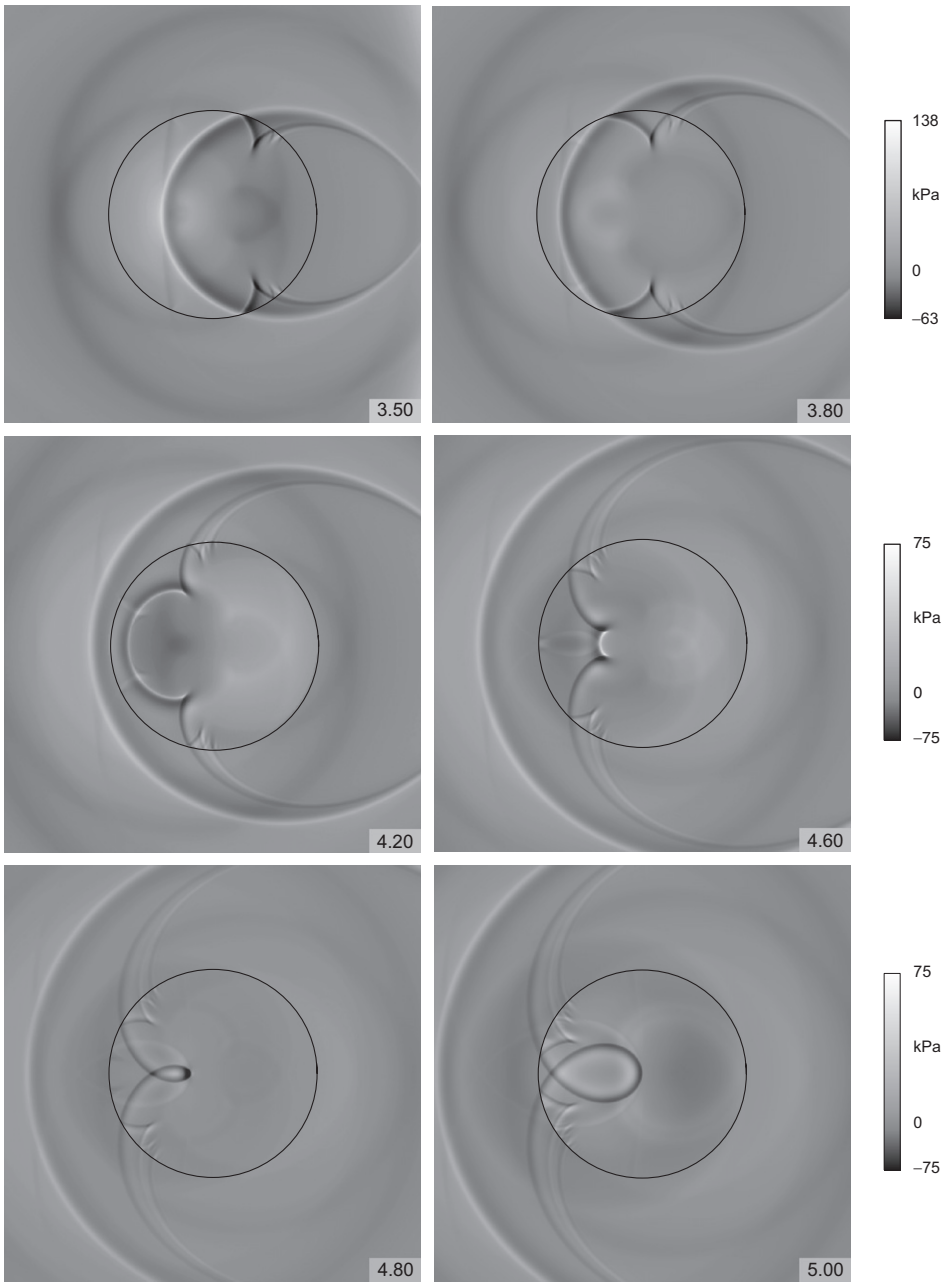

Fig. 6. (*Continued*)

Depending on the value of ζ, three qualitatively different scenarios of interaction are possible: the 'default' case of two identical fluids, $\zeta = 1$ (we will refer to this scenario as the 'sonic' one), a scenario where the acoustic speed in the internal fluid is lower than that in the external, $\zeta < 1$ (we term it the 'subsonic scenario'), and the case where the acoustic speed in the internal fluid is higher than in the external, $\zeta > 1$ (the 'supersonic scenario'). We note that the terminology suggested is, to some extent, ambiguous (we are only considering sonic waves here), but it adequately reflects the physics of the processes, and thus appears to be suitable in the present context. An extensive summary of the acoustic properties of a wide variety of fluids can be found in Ref. [38].

Throughout this section, we consider a steel shell with $h_0/r_0 = 0.01$, $c_s = 5000\,\mathrm{m/s}$, $\rho_s = 7800\,\mathrm{kg/m^3}$, and $\nu = 0.3$ submerged into water, $c_e = 1400\,\mathrm{m/s}$ and $\rho_e = 1000\,\mathrm{kg/m^3}$. The properties of the internal fluid vary depending on the scenario considered. As for the incident shock load, we consider the same large-stand-off shock wave as before (e.g. Ref. [31,33]), i.e. a shock wave with the source located at the distance of four radii of the shell from the shell's surface. As was discussed in Ref. [31], the present linear model is most suitable for modeling such a shock wave, as opposed to a close explosion for which a linear model is hardly suitable. The parameters of the wave, i.e. the rate of the exponential decay λ and peak pressure in the front p_α, were chosen to be 0.0001314 s and 250 kPa, respectively.

6. Sonic scenario ($\zeta = 1.00$)

We first address the case of two identical fluids. Even though this case has been previously addressed in much detail [31,32], only the internal field was visualized and discussed, not the entire internal-external field. As a result, the effect of the internal field on the external one was not clear. Here we eliminate that drawback, and focus on the complete internal-external analysis, and, in particular, discuss a number of interesting and sometimes unexpected features the external field exhibits in the presence of the internal fluid.

Fig. 6 shows the dynamics of the acoustic field for the shell filled with and submerged into water. (We note here that in some of the images throughout the paper, the pressure corresponding to the highest halftone in the legend (white) is lower than the actual highest pressure in the image (usually attained in a very localized region, as is the case when focusing is visualized). This has been done in order to ensure a more balanced distribution of the halftones in the respective images, and their better overall appearance.) There are several interesting features of the field that we would like to comment on. First of all, a phenomenon that only became apparent now, when the internal and external fields are visualized simultaneously. Namely, the Mach stems in the internal and external fluids are each other's geometrical continuation, and they contact the surface of the shell at the same points; the phenomenon is particularly apparent after $t = 2.00$. Fig. 7 shows the instant $t = 2.25$ separately at a larger scale, with the internal and external Mach stems labeled MSI and MSE, respectively.

This is a very interesting observation. It constitutes another, less obvious but more physically significant level of the shell's 'transparency' to a shock wave: along with the transparency in the sense that the internal wave is a geometrical continuation of the incident wave inside the shell [32], we now observe the transparency in terms of the shock wave reflection phenomena. In other words, it is almost as if the Mach stems were a

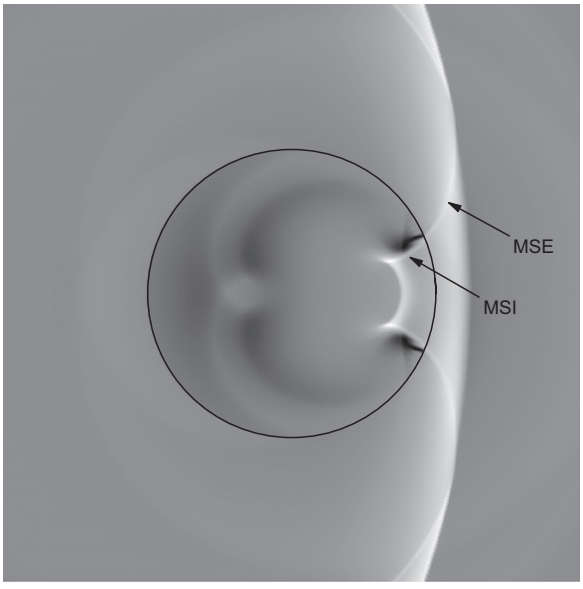

Fig. 7. Mach stem pattern at $t = 2.25$ in the sonic case of $\zeta = 1.00$.

hydrodynamic phenomenon that existed in the fluid on its own, and would merely propagate right through the 'transparent' shell without any change of shape or pressure magnitude. We also emphasize that the internal Mach stems are due to the *secondary* Mach reflection that follows the primary regular one, and the external Mach stems are the result of the *primary* reflection which is Mach. This is yet another link between the internal and external reflection processes which exhibit different types of the primary reflection for most of the process.

The connection between the internal and external wave reflection phenomena does not end with the primary Mach stems 'complementing' each other. Later in the process, the multiple regular reflection develops in the internal fluid, a phenomena which was discussed in the present context in Ref. [31], and was observed experimentally for a physically similar setup by Sun and Takayama [39], and, with a lesser degree of the setup's similarity, by Skews and Kleine [40, Fig. 9(a)]. A well-developed triple regular reflection is clearly seen at, for example, $t = 3.80$ and 5.00 (the latter waves are, in fact, the last three self-similar reflected waves of a quadruple regular reflection with the primary wave having already reflected from the shell surface). One can observe that the transition of the internal multiple regular reflection into the external fluid occurs continuously throughout the process, and is a very interesting phenomenon which could not be observed in the studies of the internal field alone.

The transition can be noticed as early as $t = 2.80$, and by $t = 3.50$, the external 'continuation' of the secondary internal Mach stems is fully developed. We emphasize that not only the geometry of the stem is preserved, the pressure sign is not changed either, and one observes regions of negative pressure of approximately the same magnitude adjacent to the shell surface. The process continues, and by $t = 3.80$ the transition of the tertiary Mach stems has occurred, reaching the fully developed state by $t = 4.20$. Finally, by $t = 4.80$, the transition of the Mach stems of the fourth-order is seen to have fully occurred.

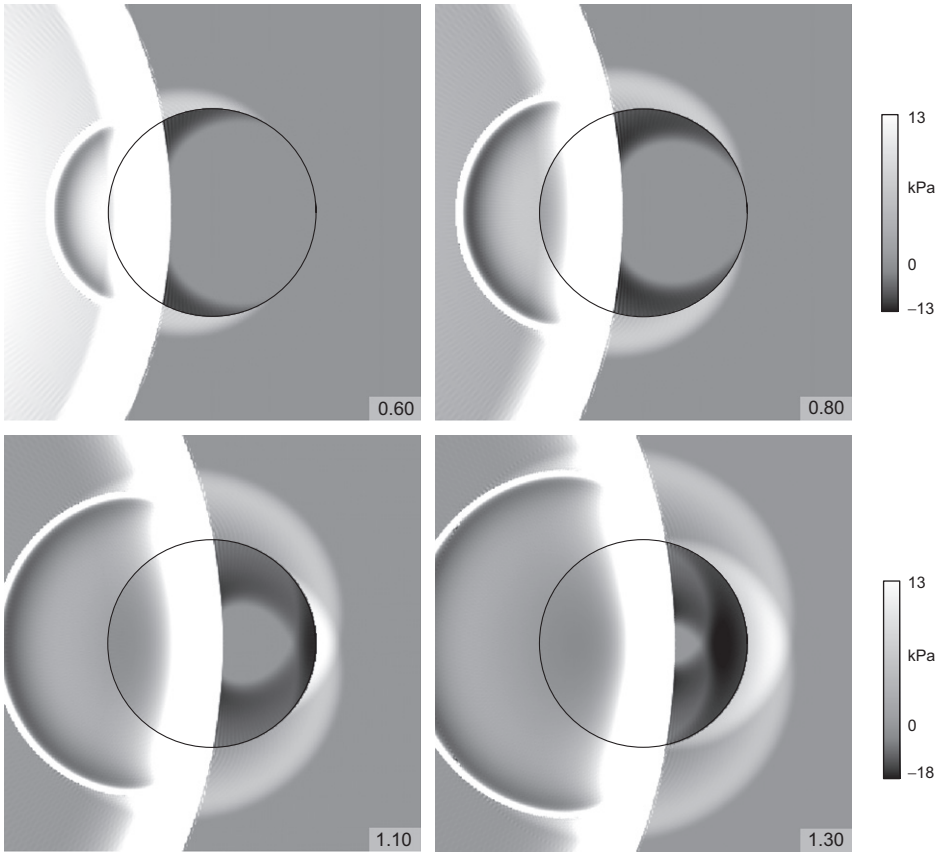

Fig. 8. Close-up of the dynamics of the shell-induced field in the sonic case of $\zeta = 1.00$.

As a result of this multiple transition process, there are four wavefronts propagating upstream behind the scattered wave, with positive and negative pressure alternating. This is yet another illustration of just how incomparably more complex the interaction is when the internal fluid is present — the only upstream-propagating wave observed due to wave reflection phenomena for a submerged evacuated shell was the scattered one [33]. It is also particularly clear now that from the acoustical point of view, a fluid-filled shell subjected to a non-stationary pulse is a much more active and 'interesting' source than an evacuated shell, an observation that is of particular importance for applications where acoustic signatures of submerged objects are a concern.

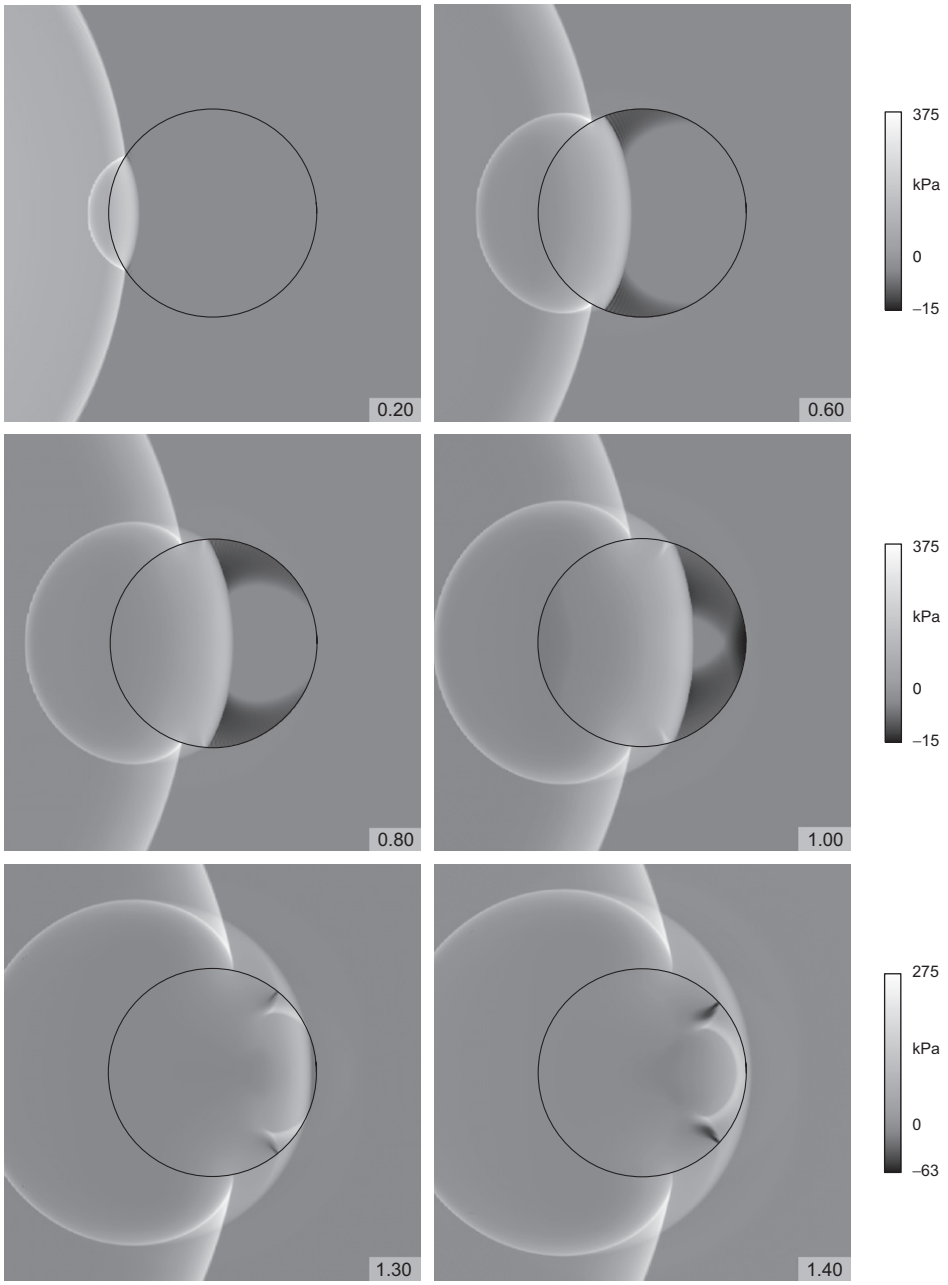

Fig. 9. Dynamics of the acoustic field in the supersonic case of $\zeta = 1.50$.

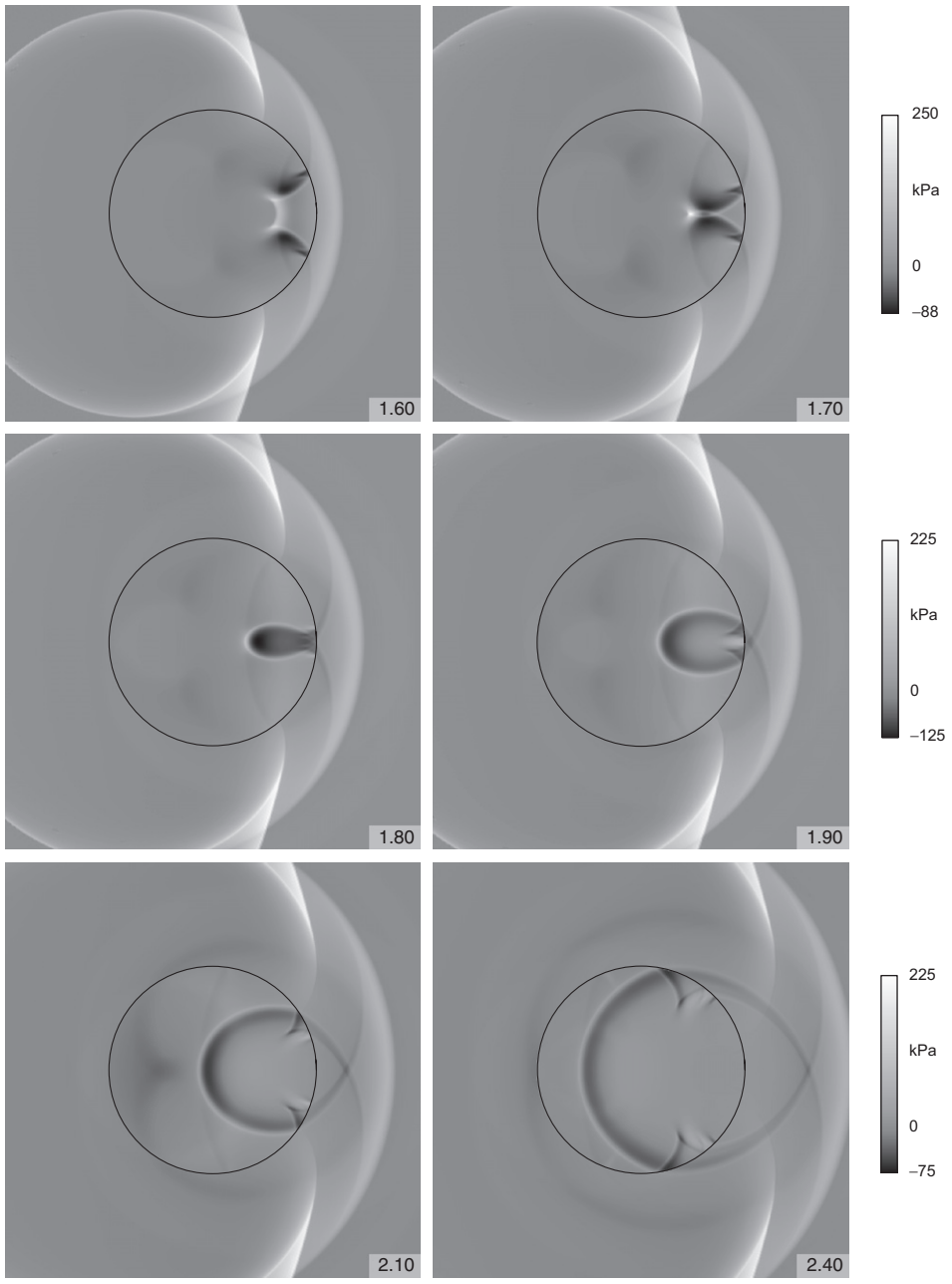

Fig. 9. (*Continued*)

We also note that, in spite of the presence of the many secondary features caused by the wave reflection phenomena discussed, the front of the incident wave remains virtually 'intact' after the incident wave passes over the shell, both in terms of its geometry and the pressure magnitude. This is not the case for an evacuated shell (e.g. Ref. [33]) where the front of the scattered wave past the shell is considerably different from what is observed in the absence of the shell, neither is it the case for any ζ other than unity, as we will see shortly.

From the practical point of view, this feature of the interaction implies that a shell filled with the same fluid as the surrounding one does not considerably change the intensity of the impact the shock wave has on structures located downstream, even when they are located quite close to the shell. This observation gives another meaning to the notion of transparency of a shell to a shock wave (introduced in Refs. [27,28] and

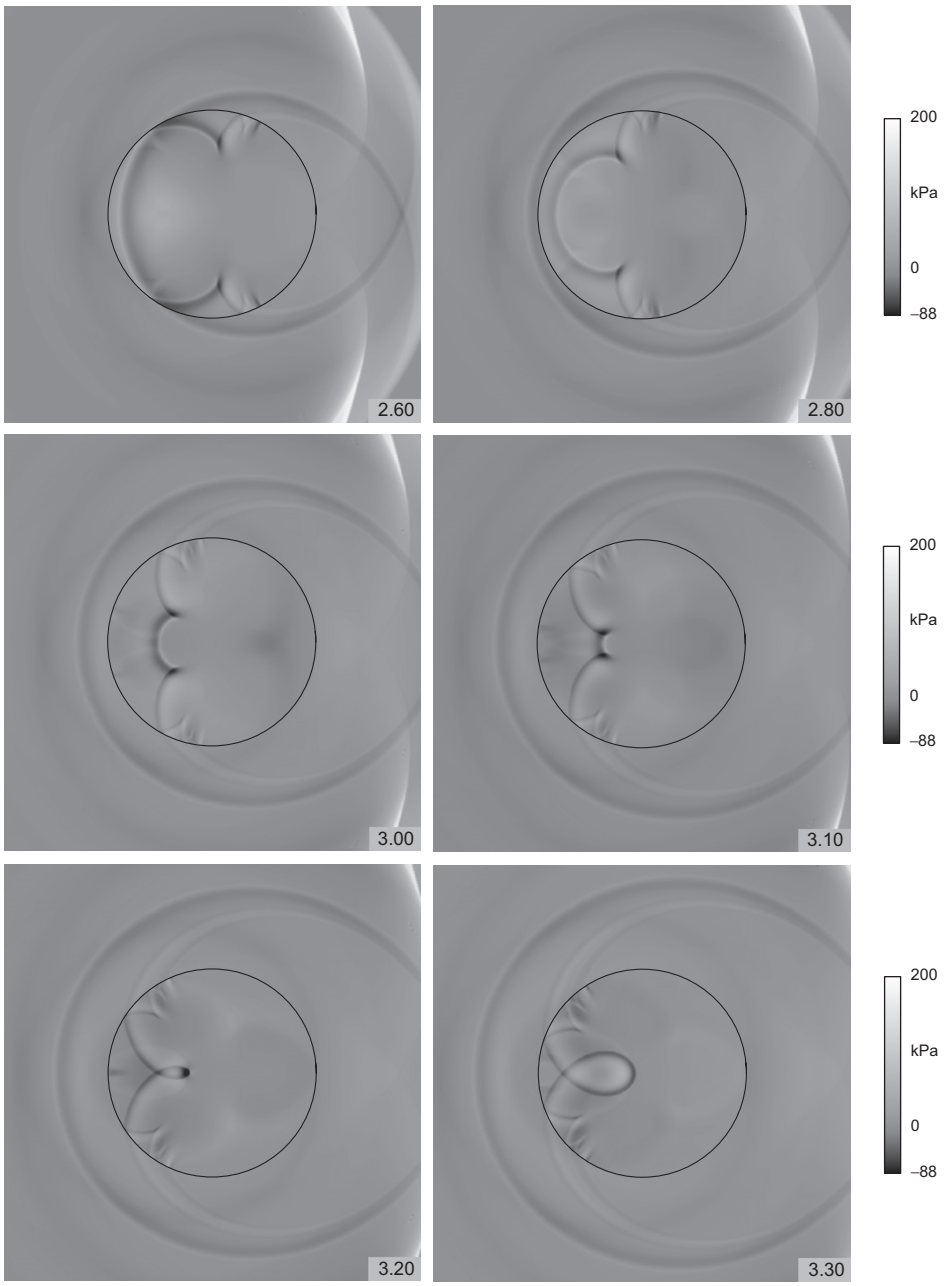

Fig. 9. (*Continued*)

further elaborated for the present case in Ref. [32]): now it is possible to talk about the 'global transparency' in a sense that a submerged fluid-filled shell does not seem to significantly reduce the shock load on structures positioned downstream, as opposed to the 'local transparency' discussed in Ref. [32] where the mechanism of the transition of the external wave inside the shell was the primary concern.

Another remark we would like to make concerns the shell-induced waves, i.e. the acoustic waves induced in the fluids by the elastic waves propagating in the shell (e.g. Refs. [21,31–33]). First of all, we note that in Fig. 6, the internal and external shell-induced fields appear to have dramatically different intensities: the former is clearly visible whereas the latter is not. This is due to the fact that the internal shell-induced pressure is negative, and is often the only negative pressure observed inside the shell at a given instant. The external

pressure, however, is positive, but is always lower in magnitude than the incident and scattered components, and as a result, it appears to be of much lower intensity than its internal counterpart. To make sure both components are shown equally well, the positive pressure range was narrowed down in Fig. 8 which shows a few selected snapshots of the early interaction.

One can clearly observe how the elastic waves propagating in the shell radiate into the fluids inducing negative pressure inside the shell and positive outside; the respective pressure has approximately the same magnitude. Since the acoustic speeds in the internal and external fluids are identical, the advancements of the waves normally to the shell surface are the same at any given point, even though the shapes of the internal and external radiated fields are obviously not. The same holds true when the circumferentially propagating elastic waves superpose at the tail point and continue to propagate upstream: the radiated fields have different geometries determined by the curvature of the shell, but the normal advancements of the waves induced by the superposition are still the same.

This uniformity of the internal and external shell-induced fields is a unique feature of the sonic interaction, and will no longer be the case when the internal and external fluids have different properties. The radiation of elastic waves into the fluids continues throughout the interaction, and is partly visible in some of the snapshots of Fig. 6. The dynamics of the complete internal-external shell-induced field is not addressed here: its physics is rather simple, even though the fields themselves are often difficult to observe due to the presence of other waves. An adequate picture of the complete shell-induced field in the sonic case can always be rendered by combining the images of the internal [31] and external [33] shell-induced fields.

7. Supersonic scenario ($\zeta > 1.00$)

It seems that there are not particularly many fluids of industrial significance that have acoustic speeds significantly exceeding the acoustic speed in water [38]. Thus, we will consider a hypothetical fluid that has the acoustic speed that only exceeds that of water by 50%, and has the same density, i.e., $c_i = 2100\,\mathrm{m/s}$ ($\zeta = 1.50$) and $\rho_i = 1000\,\mathrm{kg/m^3}$. All other parameters of the system remain the same.

The acoustic field in this case, Fig. 9, is very different from the scenario of two identical fluids. The internal pressure wave is no longer a geometrical continuation of the incident wave inside the shell, and its front, even though still convex, has the curvature that exceeds that of the incident wavefront. Much more importantly, the wave fronts in the internal and external fluids are not aligned anymore, and contact the shell at different points, the internal front being far ahead of the external one. Furthermore, not only the internal shock wave

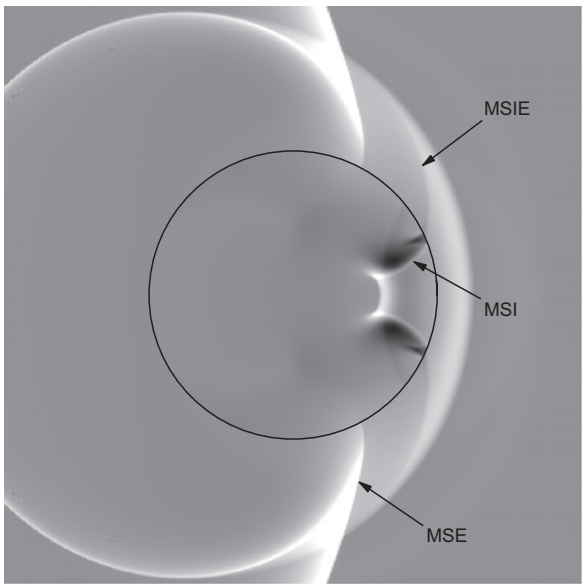

Fig. 10. Mach stem pattern at $t = 1.60$ in the supersonic case of $\zeta = 1.50$.

propagates ahead of the external one, it also 'leaks' back into the external fluid downstream inducing very significant pressure in the regions not yet affected by the incident wave. This certainly is an interesting phenomenon since now there are not one but *two* high-magnitude waves propagating downstream in the external fluid, even relatively early in the interaction — the primary scattered one, and the secondary one transmitted via the internal fluid back into the external one.

The existence of such a secondary field is also important in a different way. Namely, now we have not one but two 'head' waves propagating in the external fluid, the first one is due to the radiation of the elastic wave propagating in the shell into the fluid, and the second one is due to the radiation into the external fluid of the pressure wave propagating in the internal one. The former is still low-magnitude, while the latter is of the same order of magnitude as the diffracted-radiated waves, which is very much in contrast with the sonic scenario where the head waves were always low-magnitude. This phenomenon is of definite interest in general, but it becomes critical in applications where the exact timing of the response of the system is of importance: along with the low-magnitude response that arrives at a certain point downstream of the shell prior to the incident wave (discussed in detail in Ref. [33]), in the supersonic case there also exists a high-magnitude response that precedes the incident loading.

We note that not only the front of the internal wave 'leaks' outside the shell, the internal Mach stems do so as well (the snapshots at $t>1.30$, and also Fig. 10 where the internal Mach stems are labelled MSI, MSIE stands for their 'extension' outside the shell, and MSE stands for the Mach stems of the external reflection). However, now the Mach stems of the external reflection are no longer geometrical continuation of the respective Mach stems of the internal reflection, and one observes a discontinuity between the internal Mach stems and their external reflection counterparts. As it was the case when the fluids were identical, the multiple regular reflection taking place in the internal fluid manifests itself in the external fluid as well, $t>2.10$, in the ways that are very similar to the sonic case. We also note that the pressure patterns of the other two fundamental features of the interaction, the reflection and subsequent focusing of the internal wave, are practically identical to those observed in the sonic case, even though shifted in time, and there is no need to discuss them here.

The shell-induced fields are different as well in this case: due to the difference in the acoustic speeds in the fluids, the shell-induced waves propagate with different velocities normally to the shell surface, Fig. 11, where a low-positive pressure close-up of two sequential snapshots of the early interaction is shown.

Summarizing the analysis of the supersonic case, it appears that, even though shifted in time and de-synchronized with the incident and scattered fields, the reflection and focusing of the internal shock wave follows the same pattern as in the sonic case. The most fundamental difference, aside from the timing, is the presence of two 'head' waves of substantially different magnitudes: the low-magnitude shell-induced wave and the high-magnitude wave due to the 'transition' of the incident wave back into the external fluid through the internal one. The 'leaking' of the internal Mach stems outside the shell is definitely worth mentioning as well since now the external 'continuations' of the internal Mach stems no longer coincide with the Mach stems of

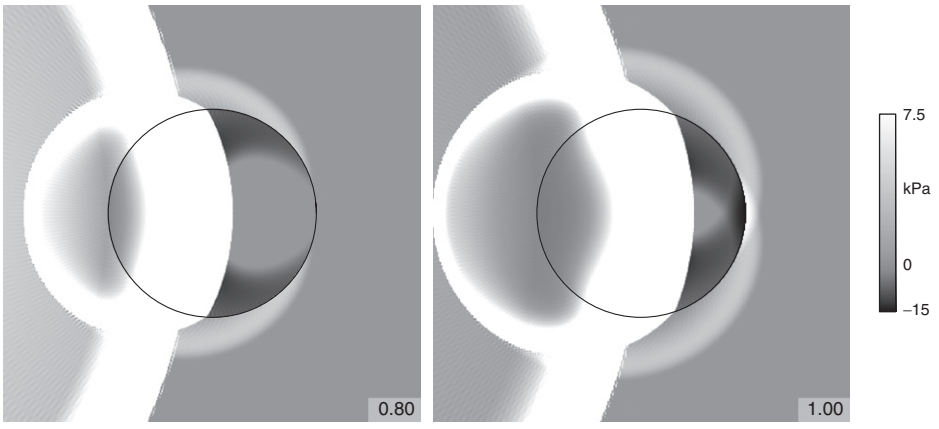

Fig. 11. Close-up of the dynamics of the shell-induced field in the supersonic case of $\zeta = 1.50$.

the external reflection. Further increasing ζ will lead to a more and more pronounced difference in the location of the fronts of the internal and external waves, and likely to the increasing curvature of the internal wavefront, but will not qualitatively change the wave pattern observed.

8. Subsonic scenario ($\zeta < 1.00$)

The subsonic scenario seems to be of greater practical relevance than its supersonic counterpart since there appear to be a larger number of fluids of industrial significance with the acoustic speeds considerably lower than that of water [38]. We will demonstrate that it is also the richest scenario in terms of the features of the acoustic field. We consider a hypothetical fluid with the acoustic velocity equal to a half of that in water, and with the same density as water, $c_i = 700\,\mathrm{m/s}$ (i.e., $\zeta = 0.50$) and $\rho_i = 1000\,\mathrm{kg/m^3}$. All other parameters of the system are the same as before.

Fig. 12 shows the dynamics of the acoustic field as the subsonic interaction develops. There are several features that make the present case fundamentally different from the two previously addressed scenarios. First of all, the front of the internal wave is no longer convex, it is concave, and has a rather complex, continuously evolving geometry. Furthermore, despite the significant difference in the acoustic speeds, the internal and external wave fronts contact the shell surface at the same point, very much unlike in the supersonic case. The physics behind such a feature of the internal wavefront is rather interesting, but not immediately apparent, and requires some elaboration.

It was shown [31] that in the sonic case, the internal pressure at the beginning of the interaction was mostly determined by the normal velocity of the shell surface moving inward. Since the propagation of the internal wave occurred at the same speed as the incident and scattered waves, the internal and external wave fronts contacted the shell surface at the same point, and exerted comparable pressure on it. In the present case the situation is different. Even though the normal velocity profile is very similar to that observed in the sonic case, due to the different wave properties of the internal fluid, the shell's motion induces a completely different internal acoustic field. Namely, there still is a high-pressure internal wave originated at the very beginning of the interaction, e.g. the snapshot at $t = 0.20$. However, now it propagates with a considerably lower velocity than the external (scattered) wave. The latter, at the same time, continues to constantly contribute to the internal field through exerting pressure on the outer shell surface, but since there is no internal front of matching geometry that exerts pressure on the shell from the inside, the external field completely determines the internal field in the proximity of the contact point.

Since the external wave propagates at a speed which is considerably higher than the internal acoustic speed, the corresponding near-surface high-pressure regions of the internal field are present far ahead of where the acoustic response of the internal fluid would be detected in the absence of the external loading. At the same time, the high-pressure wave originated at the head point at the very beginning of the interaction travels downstream at the acoustic speed of the internal fluid, and thus is far behind the near-surface regions. The result is the concave shape of the wavefront.

We therefore emphasize that, in the subsonic case, the term 'wavefront' in the context of the internal fluid becomes somewhat ambiguous: usually when one refers to the front of an *acoustic* wave, it is assumed that it propagates with the velocity equal to the acoustic speed in the medium. Here, however, we observe an acoustic wave that has a 'front' propagating with a velocity that is *perceivably* higher than the acoustic speed in the fluid (for example, the snapshot at $t = 1.10$: the internal high-magnitude pressure is detected at locations where it clearly would not be if there were no external wave). Of course, as one would expect, no laws of physics are violated here, and the seemingly non-physical behavior is purely due to the geometry of the shell: the acoustic wave itself, once originated at the surface, propagates precisely at the internal acoustic speed. The possible confusion arises from the fact that the *region itself* where the acoustic wave is induced is moving downstream with supersonic (relative to the internal fluid) velocity.

Thus, even though the situation observed can be explained rather easily, one definitely needs to be aware of it to avoid physically incorrect interpretation of the wave patterns, and from here on, when using the word 'front' for the internal wave in the subsonic case, we keep in mind the remarks made. We also note that one possible way to alleviate this ambiguity is to focus on the central, high-magnitude region of the internal front

which represents the response of the fluid at the very beginning of the interaction, and which always propagates at the acoustic velocity in the internal fluid.

The point of contact between the internal and external fronts is clearly identifiable in the lit zone ($\theta \leqslant 90^\circ$) and right after the transition into the shadow zone. As the front progresses into the shadow zone, the contact becomes less defined, and eventually (after $t \approx 2.40$) practically disappears. This is due to the fact that in the shadow zone, the external wave does not have a pressure discontinuity associated with it, and the magnitude of the pressure in it decreases considerably as well. The internal field responds accordingly, and is dominated, in terms of the magnitude, by its central part, e.g. the snapshot at $t = 2.15$. When the external Mach stems merge at the tail point at $t \approx 2.70$, the internal front closes in at the tail point as well, and the respective

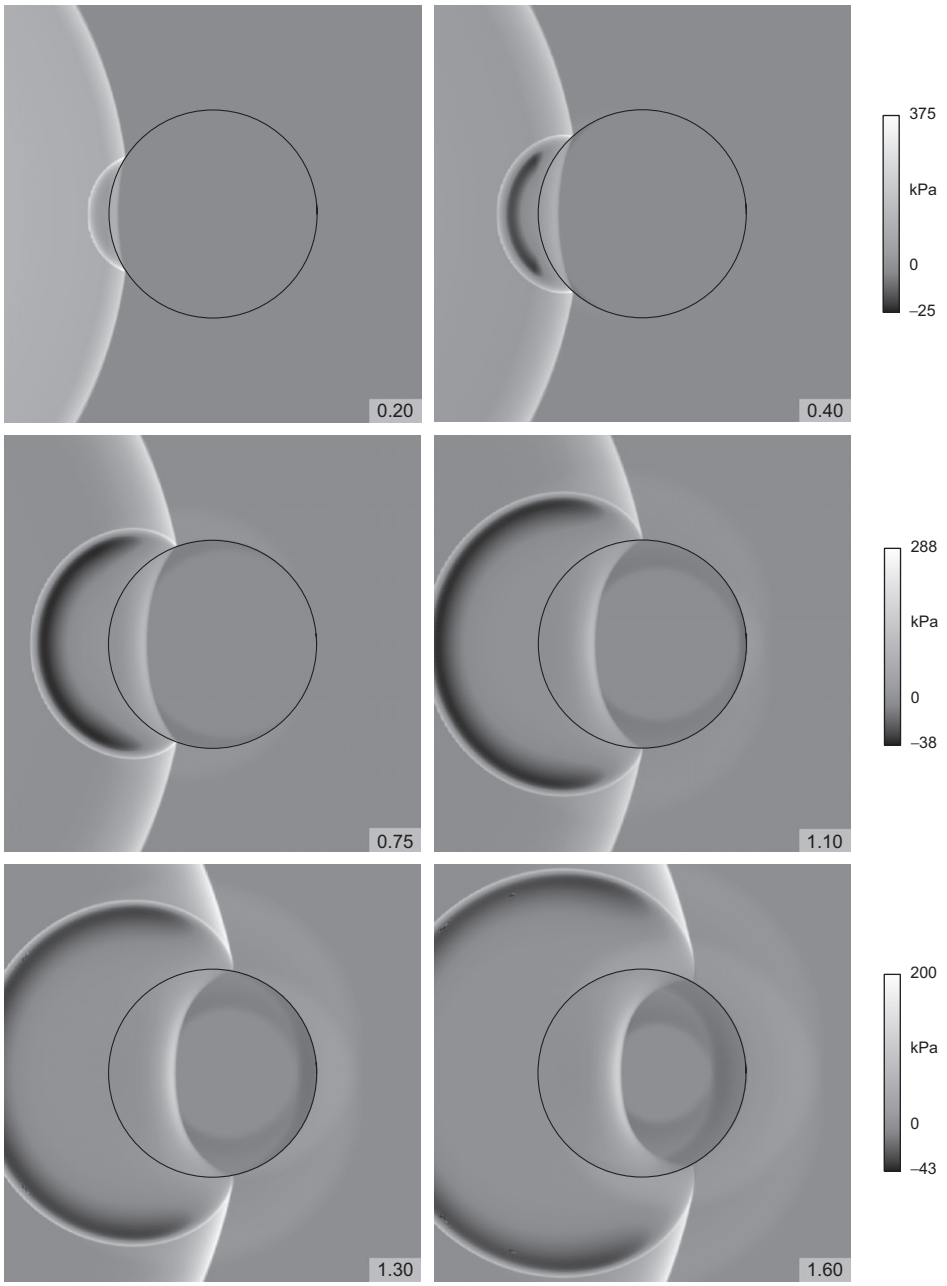

Fig. 12. Dynamics of the acoustic field in the subsonic case of $\zeta = 0.50$.

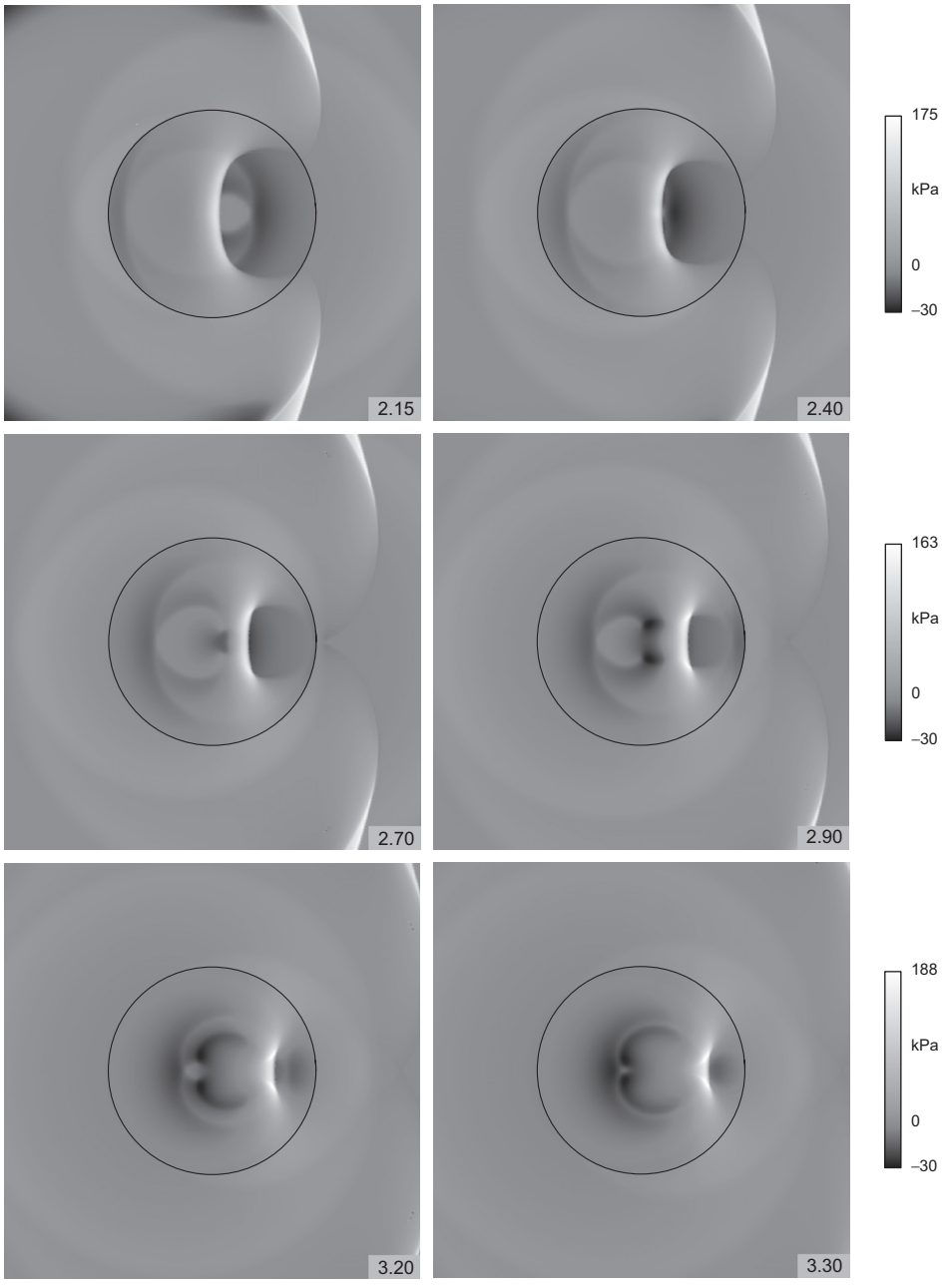

Fig. 12. (*Continued*)

radiated wave starts to propagate upstream. Such behavior, technically, appears to constitute the reflection of the internal pressure wave from the tail region. This phenomenon, however, needs clarification.

If we looked at the waves propagating in the internal fluid in the absence of the shell, they, obviously, would not cover the shell's diameter in 2.70 time units. Therefore, as was discussed earlier, the fact that the 'front' of the internal wave reached the tail point at $t \approx 2.70$ is exclusively due to the existence of the external fluid, not the wave effects in the internal one. The central part of the internal front, however, does propagate at the internal acoustic speed. Thus, to be terminologically correct and consistent with the sonic and supersonic cases, by the 'reflection' of the internal wave from the shell surface we shall mean the reflection of its central part propagating at the internal acoustic speed.

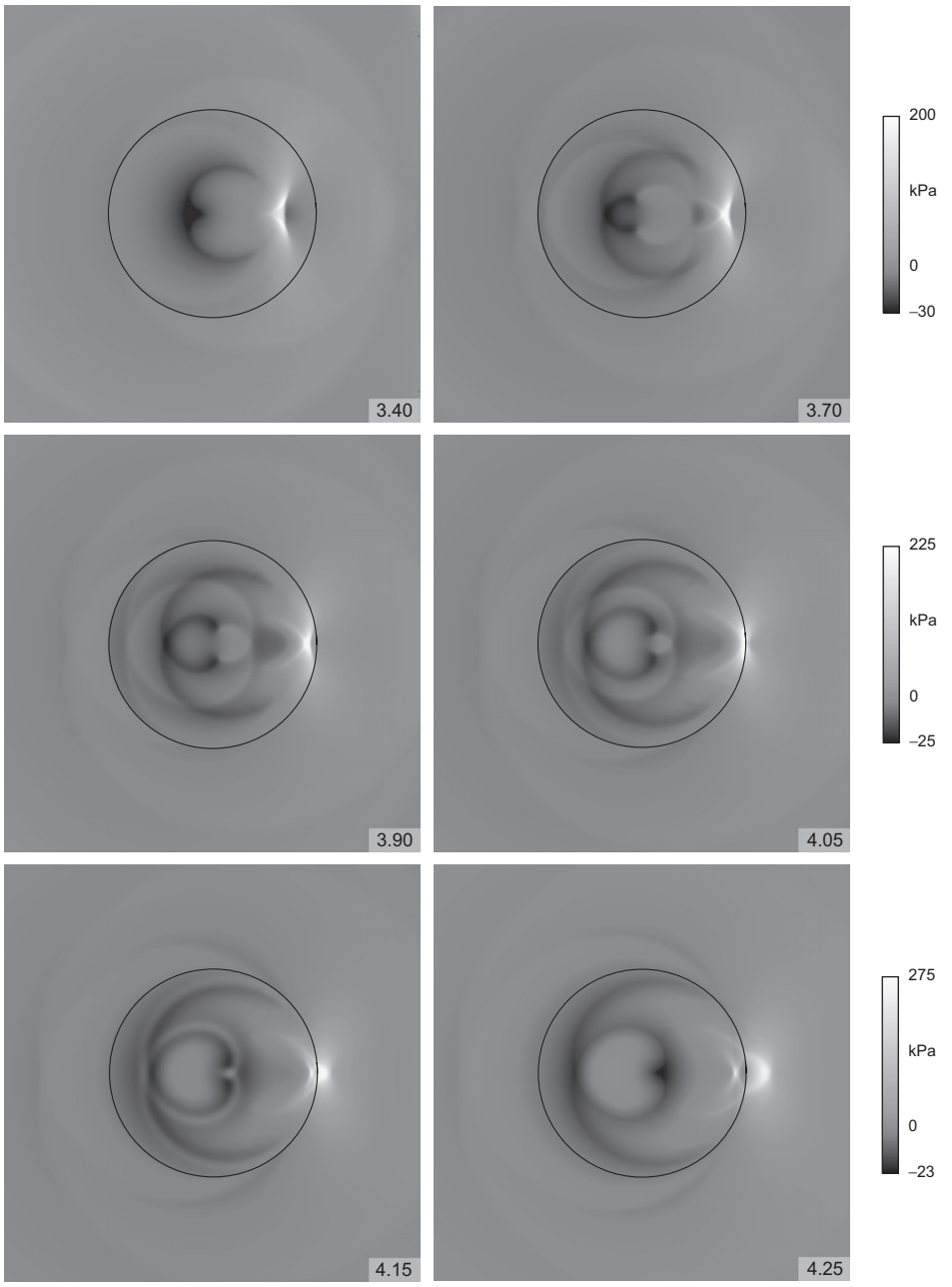

Fig. 12. (*Continued*)

We also mention that there is another fundamental difference in the physics of the internal wave in the subsonic case, at least when ζ is sufficiently small: there is no specific reflection pattern observed where the wave contacts the shell surface, neither regular nor Mach. This further supports the argument that the dynamics of the near-surface regions of the internal fluid is determined by the effects in the external fluid, not the shock wave reflection phenomena. It is also an indication that the internal wave observed in this case is not a shock wave in the classical sense but is a combination of the initial response of the internal fluid to the incident shock (the central region of the front) and the effects of the incident and scattered waves as they propagate in the external fluid (the regions in the proximity of the walls).

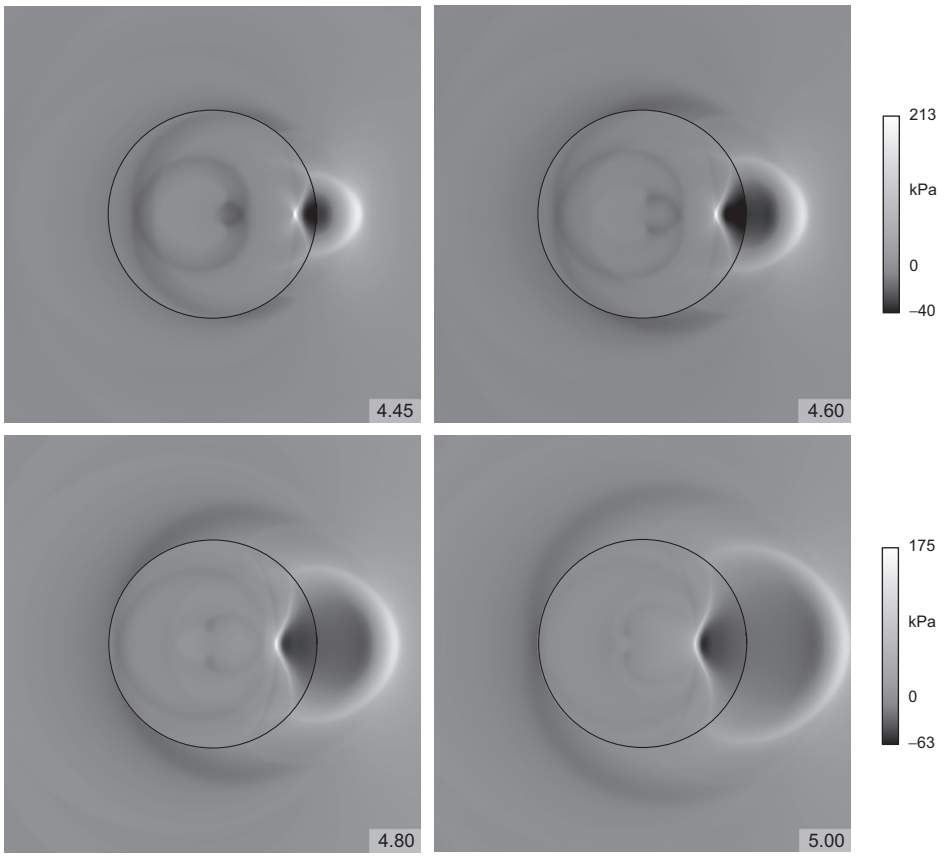

Fig. 12. (*Continued*)

The geometry of the internal front is worth commenting on as well. Almost perfectly circular (or, perhaps, parabolic) at the beginning of the interaction, it starts to exhibit a non-uniform curvature later on ($t \approx 1.00$), becomes apparently non-circular by $t \approx 2.00$, and by $t \approx 2.40$, it takes on an almost rectangular-like shape. After the near-surface regions of the front merge at $t \approx 2.70$ (about the same time when the Mach stems of the secondary reflection merge in the sonic case), they begin to propagate upstream. Meanwhile, the central region of the front is still propagating downstream, and after $t \approx 2.80$ starts to disintegrate into three distinct parts, two high-magnitude ones and one lower-magnitude. Eventually ($t \approx 3.30$), the regions propagating upstream and downstream collide, resulting in the V-shaped (the snapshot at $t = 3.40$) and later almost X-shaped ($t = 3.70$ and 3.90) high-pressure formation propagating downstream.

During this stage of the process, the pressure in the high-magnitude formation mentioned increases very considerably, and at $t = 3.90$, for example, it exceeds the peak incident pressure, p_α, by more than 25%. Such high pressure attained in such a localized region certainly constitutes focusing, and its existence so late in the interaction is alone sufficient for one to be particularly concerned with the subsonic scenario. Shortly after the focusing occurs, the high-pressure region falls on the shell surface and reflects from the tail region. This corresponds to the instant when the central region of the internal wavefront finally reaches the tail point, and thus constitutes the reflection of the internal wave in the classical sense. The pressure rise associated with the reflection is detected as well, and the peak reflection pressure exceeds the maximum incident one by more than 100%, $t = 4.06$. The practical significance of such pressure rise is obvious, and it should be particularly emphasized that by the instant in question, not only the incident wave has moved over the shell, its front has moved the shell's diameter away from the structure.

We would also like to emphasize two other aspects here. First, the focusing observed occurs *before* the central region of the internal wave front reflects from the tail region of the shell. This fact constitutes an

essential difference between the present and sonic reflection and focusing mechanisms, and is of definite theoretical interest (in the sonic case, the reflection of the internal wave from the tail region preceded the focusing [31]). Second, it so happens that, in the chosen scenario of $\zeta = 0.50$, the focusing occurs very close to the shell surface, and there is not enough time to observe the evolution of the post-focusing pressure pattern before reflection from the shell surface takes place.

We also note that it is somewhat difficult to pinpoint the precise spatial and temporal location of the focusing: the pressure is high and of approximately same magnitude during a finite time interval preceding the reflection (approximately [3.85, 3.95]), without a distinct peak at any particular point. The geometry of the respective high-pressure region is not too helpful here either — it is approximately X-shaped with the highest pressure in the middle for a relatively long time, with no particular instant standing out. Thus, discussing the timing of the focusing in this case, it probably makes more sense to talk about the focusing interval, not a specific focusing instant. The magnitude of the focusing pressure, however, can be determined quite accurately, with less than 5% error.

From the practical point of view, the possible negative effects of the high focusing/reflection pressure are worsened by the fact that it is sustained for a relatively long time. Specifically, it exceeds the peak incident pressure when $t \approx 3.70-4.15$, which is more than 20% of the incident wave passage time (i.e., the time it takes for the incident wave to move over the shell).

The unique features of the subsonic scenario are not limited to the occurrence of the focusing prior to the reflection from the tail region. After the reflection, the reflected wave starts to propagate upstream, and a region of negative pressure emerges behind its front, $t \approx 4.30$; the front is W-shaped by that time, with a distinct pressure peak at the center. The negative pressure in the region in question can be quite low, up to 20% in magnitude of the peak incident pressure. Moreover, the region is quite extensive, and exists for a long time, $t \approx 4.30-6.00$, or 85% of the incident wave passage time. This, once again, demonstrates that the present scenario is completely different from the sonic one where high-magnitude negative pressure did exist late in the interaction, but was very localized, and was observed for a very short time. Furthermore, the existence of the extensive regions of low pressure would certainly be a significant concern if the possibility of cavitation were investigated.

There is another phenomenon of definite interest that takes place after the reflection of the internal wave from the tail region. Namely, at $t \approx 4.30-4.50$, there is another very localized region where the pressure is very high; in fact, it is so high that it exceeds the peak incident pressure by about 10% at $t = 4.46$ (clearly visible in the snapshot for $t = 4.45$). This, again, constitutes focusing, but this time, it succeeds the reflection. We, therefore, can conclude that in the subsonic case, there can occur *not one but two focusings*, one *before* the reflection, and one *after*. The fact that the second focusing occurs so late in the interaction is yet another reminder that the late interaction in the subsonic case definitely needs to be closely monitored when one is concerned about high pressure. We note that the post-focusing wavefront is bell-shaped, not ellipsoidal as was the case for the sonic scenario, and the transition from the pointed to bell shape occurs shortly after the second focusing, at $t \approx 4.50$. The difference observed is particularly striking if one recalls that the geometry of the reflecting surface did not change, only the parameters of the medium.

We note that most of the remarks made so far concerned the internal field. There, however, is an important feature of the external field that is unique to the subsonic interaction. Namely, the reflection of the internal wave from the tail region induces high-pressure region in the external fluid adjacent to the shell surface at $t \approx 4.10-4.15$, which develops into a pressure wave that propagates downstream, with a clearly defined 'front' and the subsequent pressure drop behind it. We emphasize that the word 'front' appears in quotations marks since the wave observed is not a shock wave in the classical sense — there is no pressure discontinuity associated with it. Its effects, however, are virtually the same as would be those of a shock wave originated at the tail point, at least as far as the practitioner is concerned.

The existence of this pressure wave is of importance for two reasons. First, the specifics of the interaction in the present case are such that the external fluid adjacent to the tail region does not experience significant pressure rise throughout the entire interaction up until the instant in question. Second, from the practical point of view, the wave pattern observed implies that, effectively, two shock waves are seen to propagate in the external fluid downstream of the shell, i.e., along with the primary (scattered) wave, a secondary shock wave is observed as well. It exists very late in the interaction — even at $t = 5.00$ it is clearly detectable (i.e. at the times

when the incident wave passed the shell by one and a half of its diameter), and the pressure in its front is high enough for one to be concerned about the wave's effects. This interesting feature of the interaction becomes critically important when the effect on the secondary structures located downstream of the primary shock-responding one is analyzed, or when the timing of the system's response is a concern. We particularly emphasize that the pressure in this external wave is very high during the early stages of its existence ($t = 4.10-4.30$): it exceeds p_α by almost 30% at $t = 4.10$. This is very much unlike the sonic case where the external pressure in the region adjacent to the tail point never exceeded the peak incident pressure, and is yet another unique feature of the subsonic interaction.

We also mention that the high-magnitude 'fronts' of the reflected internal and the reflection-induced external waves contact the shell surface at the same points (compare the snapshots for $t = 4.45$ and 4.60), so there is, once again, a clear connection between the internal and external wave reflection phenomena, even when it comes to secondary waves and the very late interaction. We also note that, from the practical point of view, the diversity of the effects observed implies that under the subsonic scenario of interaction, the shell remains a very active acoustic source long after the incident wave has passed over it.

Another important difference in the acoustic fields concerns the shell-induced waves, Fig. 13, where a narrower positive pressure range is shown to ensure an adequate appearance of the low-magnitude external radiated waves; only a few representative snapshots are included. The shell-induced waves still have the same velocity of propagation along the shell surface, but the velocity of propagation normally to the shell surface inward is different from that outward: unlike the sonic and supersonic cases, the normal advancement of the internal shell-induced waves is much slower than that of the external ones. The same also applies to the shell-induced pressure patterns observed after the superposition of the elastic waves at the tail point. Even though certainly an interesting phenomenon, such a difference in the velocity of propagation of the shell-induced

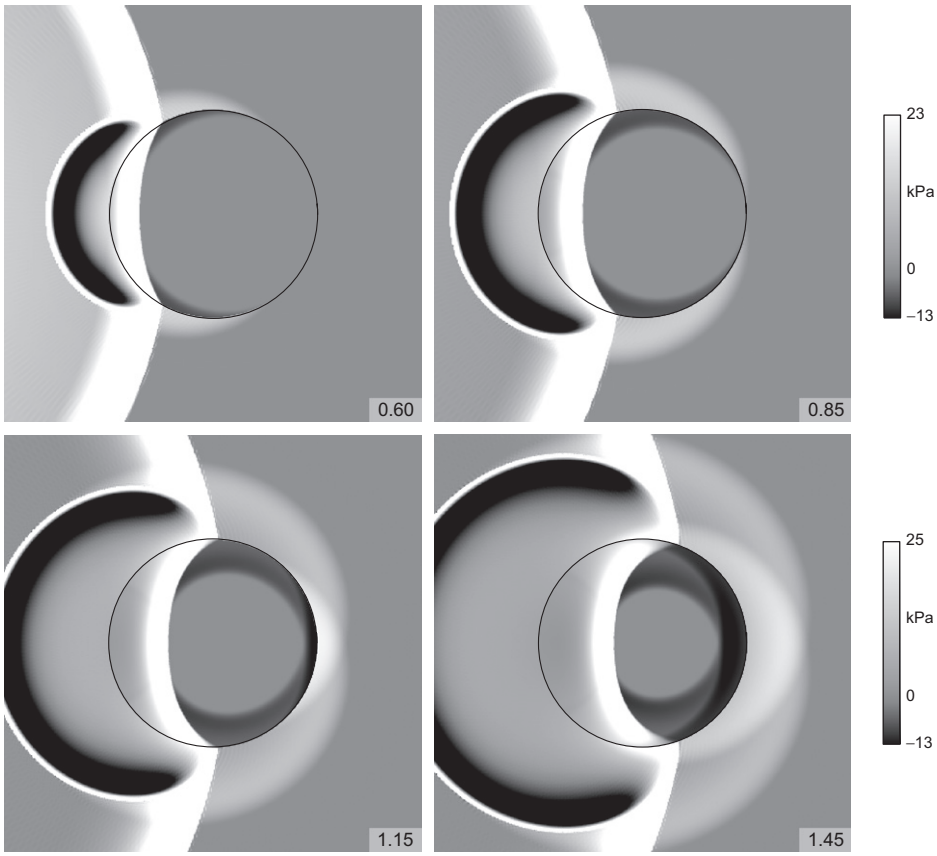

Fig. 13. Close-up of the dynamics of the shell-induced field in the subsonic case of $\zeta = 0.50$.

waves does not constitute a qualitative difference in the physics of the radiation: as long as the shell remains the same, the timing of the superpositions of the elastic waves does not change, neither does the number of passages of the waves around the shell in any given time interval.

We note that since for low values of ζ it takes much longer than four dimensionless time units for the internal wave to reflect from the tail region and return back to the head point, the usual time span considered ($0.00 \leqslant t \leqslant 5.00$) is not always sufficient to adequately represent the process. For that reason, Fig. 14 shows the very late ($5.00 \leqslant t \leqslant 10.00$) evolution of the internal field for the case of $\zeta = 0.50$ (only the internal field is shown). One can see that even though the very general features of the process are still the same as in the sonic case (propagating upstream and reflecting from the head region), the pressure patterns are quite different. We emphasize that the process is still very phenomenologically rich: for example, yet another focusing is observed at $t \approx 9.30$, and the Mach stems are clearly detectable at $t = 7.50$. Of particular interest is the fact that this complex features of the acoustic field are observed at the instants when the incident wave has passed over the shell and moved away from it by at least one and a half of the shell's diameter, i.e. the times that would certainly be deemed 'uninteresting' for the case of an evacuated shell.

Analyzing the focusing and reflection in the present case, the following needs to be emphasized. For the considered ratio of the acoustic speeds, the first focusing occurs almost at the shell surface. This, however, is not always the case, and as ζ changes, the location and timing of the focusing will change as well. Even though this is a rather obvious conclusion, is not clear at all exactly how the focusing pattern changes with ζ. To clarify the issue, we look at two more subsonic interactions, $\zeta = 0.36$ and 0.64, the acoustic speeds of 500 and 900 m/s, respectively, and analyze the dynamics of the pressure patterns observed. Since we are concerned here

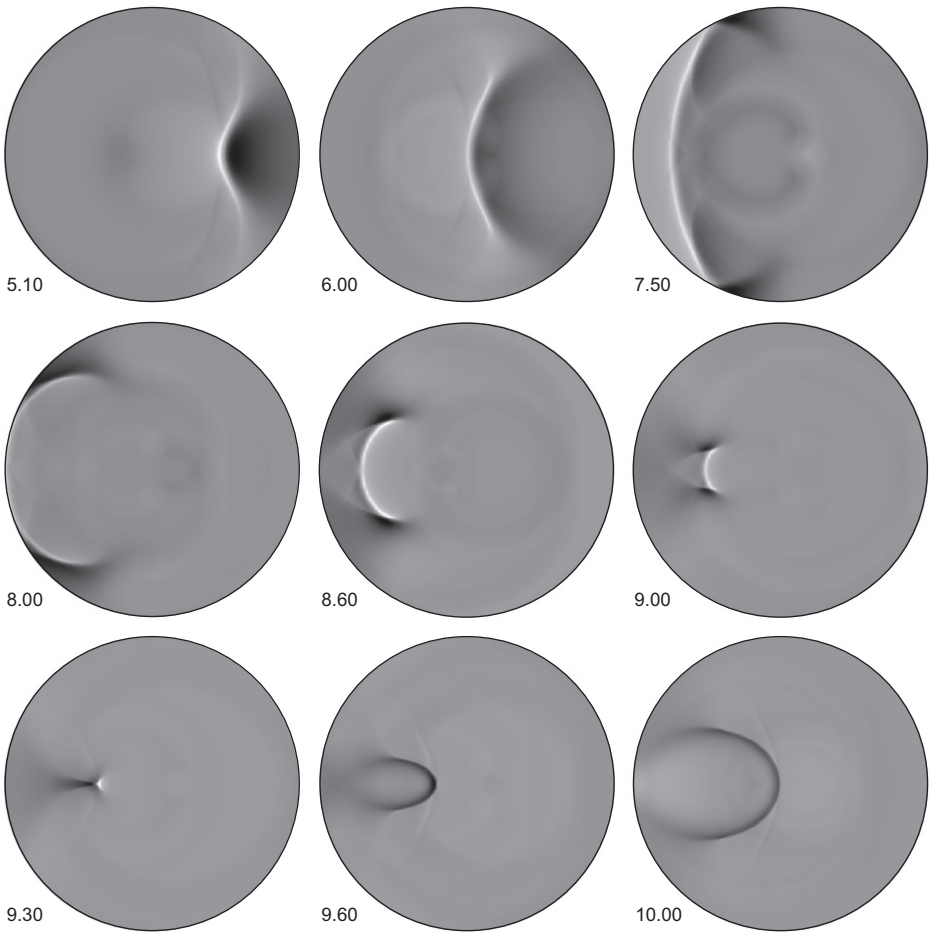

Fig. 14. Late interaction in the subsonic case of $\zeta = 0.50$.

with the focusing and reflection inside the shell, the external field is not important in that context, and we only visualize the internal field, and only do so for the relevant time intervals. Since the geometry of the pressure patterns is our primary concern here, the halftones are assigned individually in each of the snapshots to ensure their optimal appearance.

In the case of $\zeta = 0.36$, Fig. 15, the first focusing occurs at a considerable distance from the shell surface at $t = 4.48$, with high focusing pressure exceeding the peak incident one by about 30%. The post-focusing wave pattern has time to develop sufficiently before the reflection from the tail region starts at $t = 5.60$ resulting in another localized high-pressure region with pressure exceeding p_α by about 15% at $t = 5.63$. As was the case

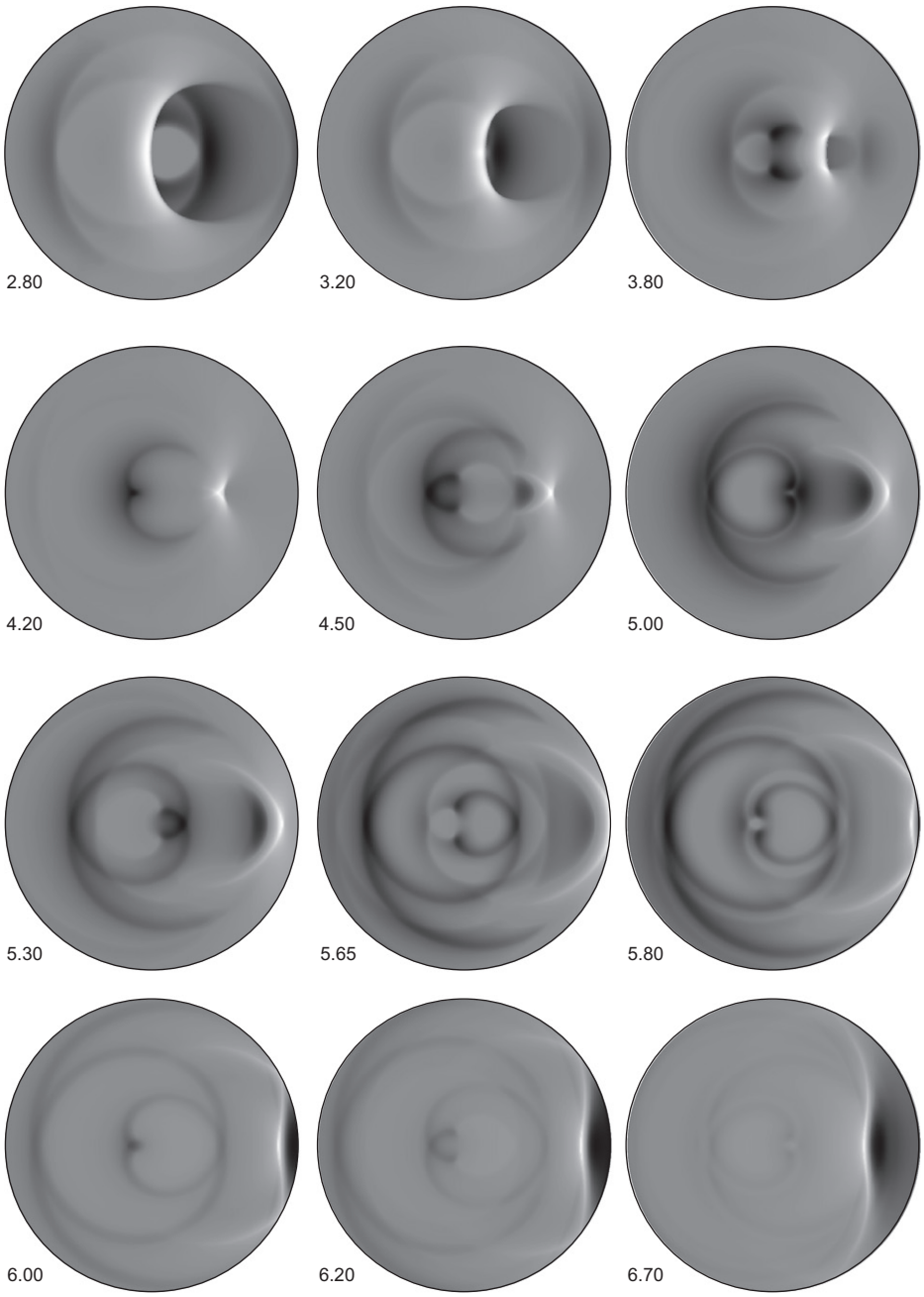

Fig. 15. Focusing and reflection for $\zeta = 0.36$.

for $\zeta = 0.50$, the maximum pressure between the focusing and reflection remains quite high — it never drops below 75% of p_α, although now the two phenomena are clearly separated. After the reflection occurs, the reflected wave propagates upstream with a distinct localized region of high pressure of about 50% of p_α attained between $t = 5.95$ and 6.10. Even though such behavior certainly constitutes second focusing, we emphasize that, for such a low value of ζ, the pressure peak in question is attained not at a point but along a finite segment of the internal wavefront, and its exact timing is difficult to pinpoint since the pressure is approximately the same during the finite time interval mentioned.

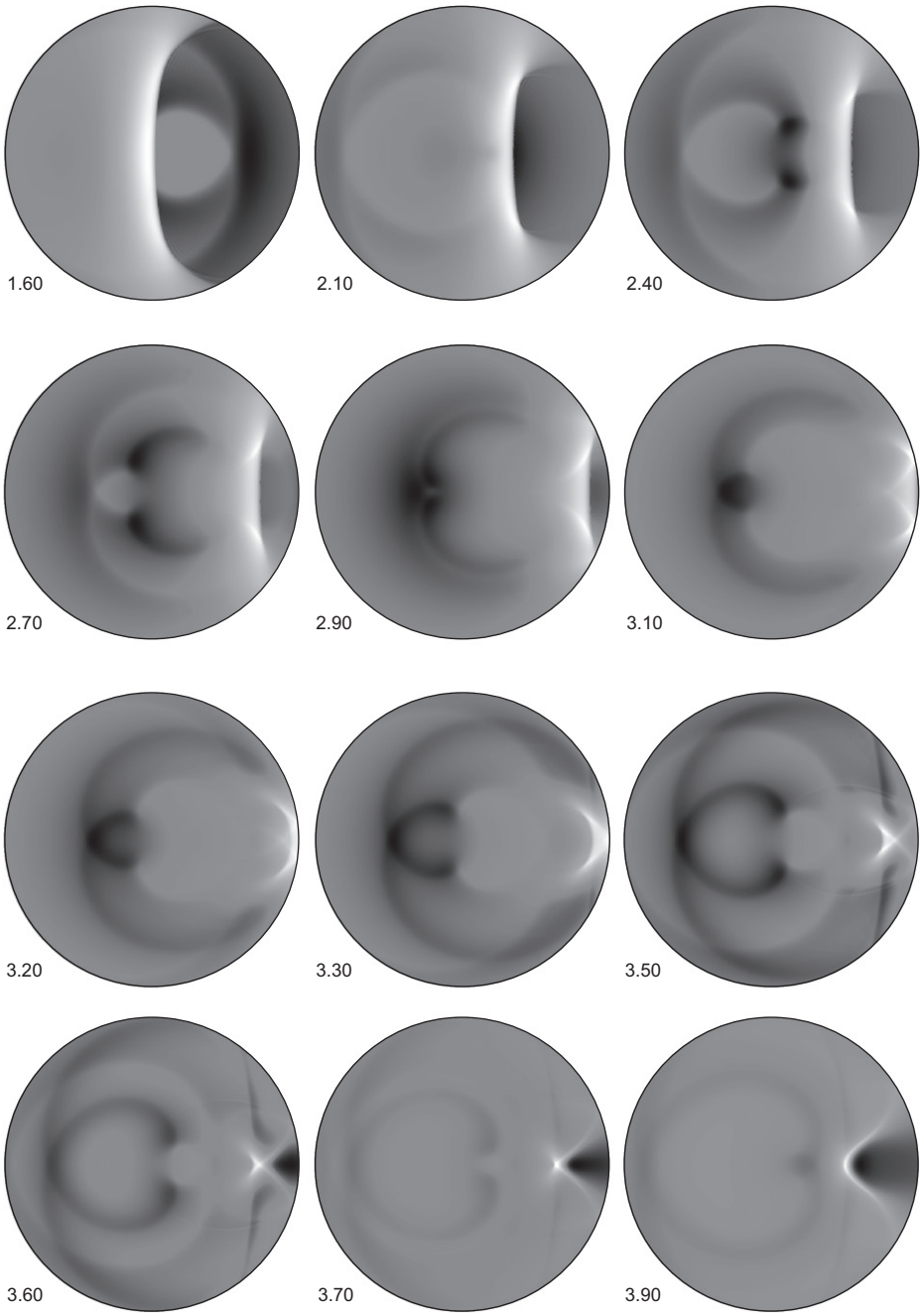

Fig. 16. Focusing and reflection for $\zeta = 0.64$.

In the second case, $\zeta = 0.64$, Fig. 16, the internal acoustic speed is high enough so that no focusing prior to the reflection from the tail region is observed, and the first peak pressure (exceeding p_α by about 20%) at $t = 3.19$ is due to the reflection. The post-reflection focusing, however, is still clearly observed at $t = 3.70$, with the peak pressure exceeding p_α by about 40% . Thus, for this relatively high value of ζ we observe the well-familiar 'reflection-focusing' mode of interaction inherent to the sonic scenario, even though the pressure pattern is still very different from the sonic case.

We have therefore established that, depending on ζ, the subsonic case itself can follow two qualitatively different sub-scenarios: one where the focusing occurs both *before* and *after* the reflection from the tail region (we term it the 'FRF mode'), and one where the focusing only takes place *after* the internal wave reflects from the tail region (the 'RF mode'). There exists a transitional mode where the first reflection and focusing occur simultaneously. The critical value of ζ separating the two modes, FRF and RF, is approximately 0.52, and any ζ in the close proximity of this critical value will yield almost simultaneous reflection and focusing. The existing of these two distinct modes of interaction with the transitional mode separating them is yet another indication of the uniqueness and complexity of the subsonic interaction, and yet another reminder of the need for a comprehensive design-stage analysis of systems involving two fluids with significantly different properties.

We note that, as was discussed when the focusing in the sonic case was addressed [31], knowing the location of the high-pressure regions is of particular practical importance when internal elements are placed inside a fluid-filled shock-responding shell (secondary pipes, equipment, etc.). This is even more so in the present case where focusing could happen not once but twice. The good news is, however, that there are regions of the internal fluid that seem to never experience particularly high pressure throughout the entire interaction, for example, for $\zeta = 0.50$ those defined by $\theta \in [\pm 135^\circ, \pm 150^\circ]$ and $r > 0.60$. Thus, when the prevailing direction of the shock loading is known, it is possible to place the internal elements inside the shell in such a way that the adverse effects of the shock on them will be minimized.

It is also interesting to point out that because during the early interaction the front of the internal wave is concave for $\zeta = 0.50$ and convex for $\zeta = 1.00$, the transition from one shape to the other is expected to occur somewhere between those two values. Specifically, it seems reasonable to expect that there exists a value of ζ such that the shape of the front of the internal wave is very close to a straight line (something very similar to what one would observe for the case of a plane incident wave under the sonic scenario). Fig. 17 demonstrates that this is indeed so: several snapshots of the acoustic field at $t = 1.10$ are shown for different values of ζ, and the transition from a concave to convex wavefront is seen to occur at $\zeta \approx 0.86$, with the only exception being the close proximity of the shell surface. Even though the shape of the internal wavefront does not seem to have any practical importance, the feature observed appears to be of theoretical interest.

Another interesting feature worth mentioning here is that for very low values of ζ, the shell-induced waves propagate in the internal fluid with such a low (relative to the acoustic speed in the shell) velocity that their inward advancement normally to the shell surface in the lit zone and the tail region are comparable, e.g. $\zeta = 0.21$, Fig. 17. The result is the formation of a narrow, almost ring-like region of negative pressure adjacent to the shell surface, with the pressure in it having similar magnitude throughout. This is an interesting phenomenon on its own, but it is of particular practical significance when cavitation is a concern: it appears that if the pressure in the region in question falls below the cavitation threshold, the separation of the shell and fluid will occur along a very significant part of the shell's circumference, and after the collapse of the cavitation zone, at least a half of the shell will experience reloading.

9. Benchmark plots

All the images presented so far have been those of two-dimensional pressure fields. However, if one intends to use the solution developed to produce benchmarks for verification of numerical codes, two-dimensional plots are not always suitable (they allow one to see the overall dynamics of the process very well, but are limiting when exact numerical values are of interest). Thus, traditional one-dimensional plots are certainly welcome here as well, and are the subject of this section.

Although a 'cylindrical' incident shock wave (with its advantages and limitations outlined above) has been considered to produce the two-dimensional images, here we will be using a plane incident wave with the same

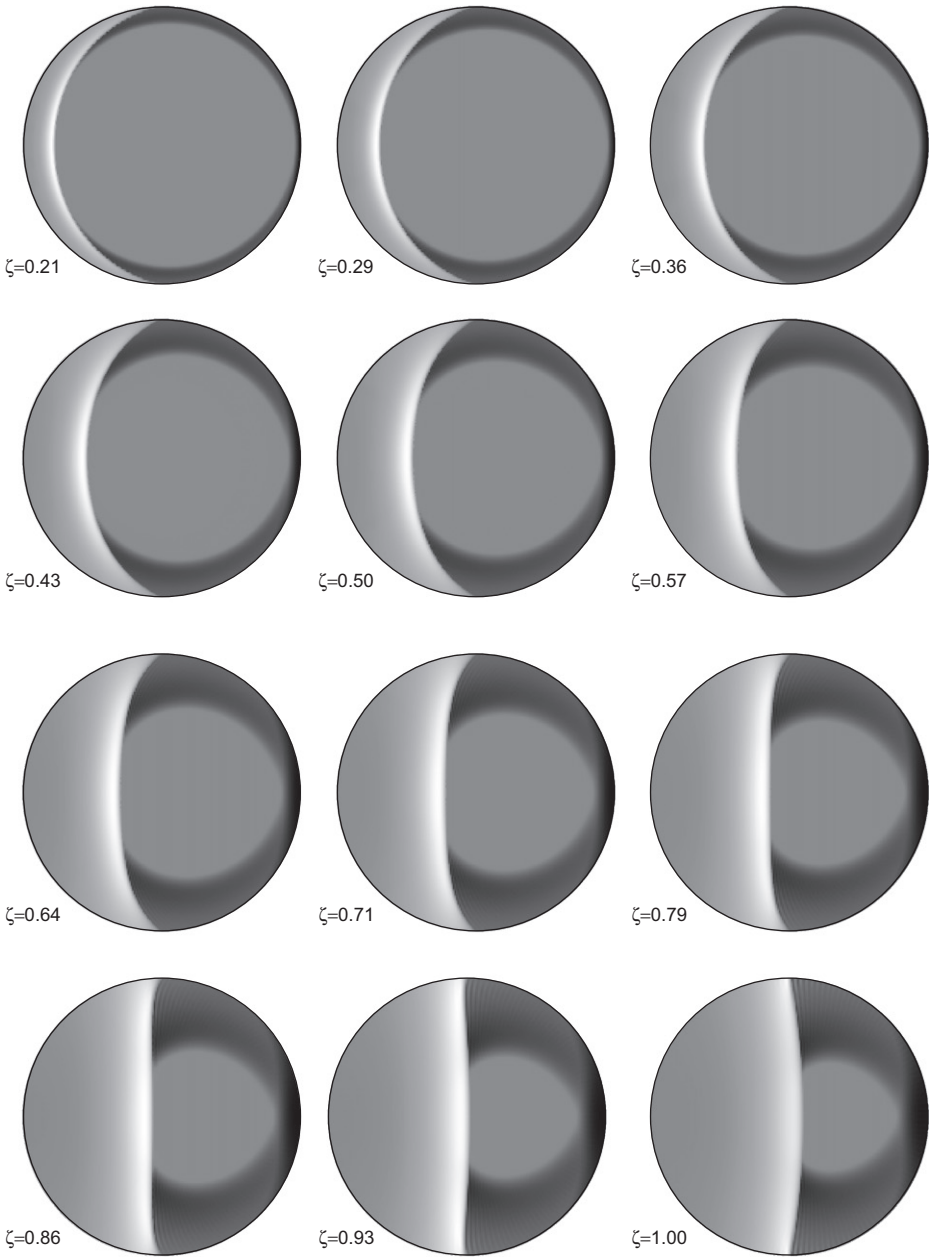

Fig. 17. Transition of the shape of the internal wavefront from concave to convex as ζ increases.

rate of exponential decay and the same pressure in the front. Although the results produced by such a wave will be less resemblant of what is seen for a three-dimensional shell and a spherical incident wave, this still appears to be a reasonable choice since a plane wave has no physical inconsistencies associated with it, and thus is more suitable as a test loading. Furthermore, a plane incident wave was used in the study by Geers [3] that largely inspired the author to adopt the approach introduced in that work to the simulation of the internal hydrodynamic fields. That, in turn, led to the present work. The plane wave is assumed to have the same parameter as before, i.e. the pressure in the front of 250 kPa and the exponential decay rate of 0.0001314 s.

Two functions were chosen for the benchmark plots. First, we plot the hydrodynamic pressure at two points on the outer structural surface (the head and tail points) for three values of ζ considered in this study, $\zeta = 0.50$,

1.00, and 1.50, Fig. 18. No noise filtering was applied in this case, and the graphs represent the 'raw' result of the summation of the respective series, thus retaining all the errors due to the series convergence. This is intended to demonstrate the limitations of the solution developed when it is necessary to obtain extremely accurate results, but also, and more importantly, to show that the error due to the series convergence is very small in the present case, and even the direct series summation results in near-perfect curves.

We note that the difference between the curves for different ζ is much more dramatic at the tail point than at the head one. This is not surprising at all since what we see at the head point is mostly determined by the initial response of the system, and is not significantly influenced by the wave propagation and reflection phenomena

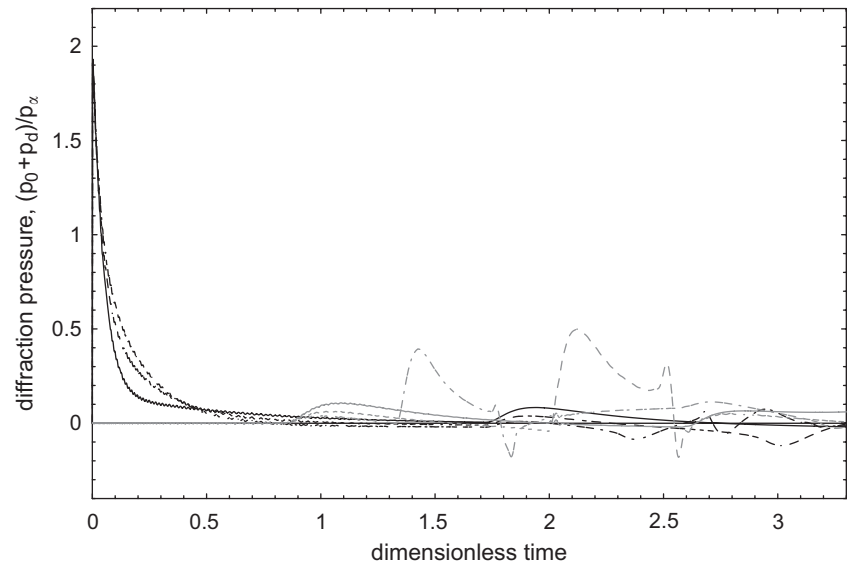

Fig. 18. External pressure at the head point (black curves) and tail point (gray curves); $\zeta = 0.50$, solid lines; $\zeta = 1.00$, dashed lines; $\zeta = 1.50$, dashed-dotted lines.

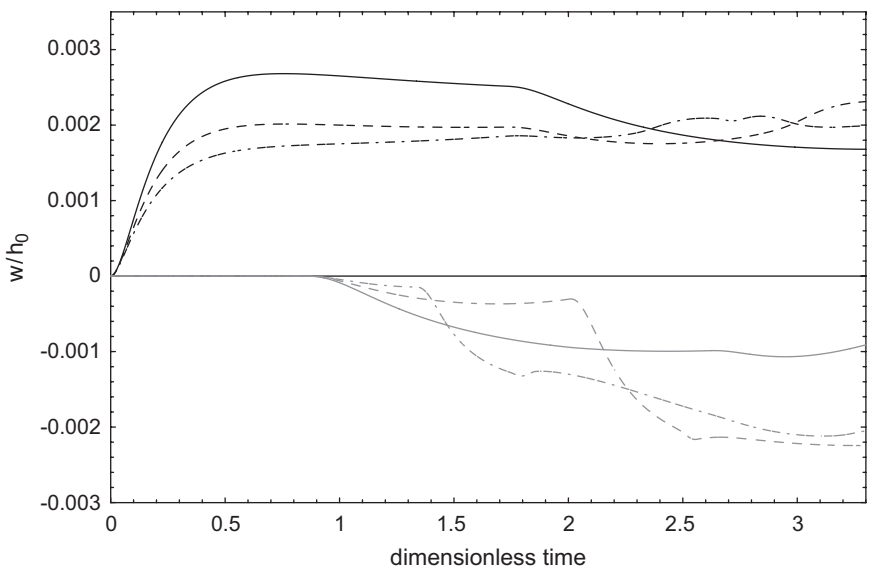

Fig. 19. Normal displacement at the head point (black curves) and tail point (gray curves); $\zeta = 0.50$, solid lines; $\zeta = 1.00$, dashed lines; $\zeta = 1.50$, dashed-dotted lines.

in the internal fluid. The tail point is completely different in that sense — the arrival of the internal pressure wave at the tail point plays a determining role in what the pressure time-history looks like there. Since for different ζ we have considerably different times of arrival of the internal wave, the plots look very different as well. The only time internal where the plots are qualitatively similar is between $t = 0.87$ (the time of arrival of the elastic waves circumferentially propagating in the shell) and the time of arrival of the internal wave for $\zeta = 1.50$. During this interval, the pressure is determined by the elastic waves propagating in the shell, not the wave phenomena in the fluids.

Fig. 19 shows the normal displacement of the shell surface at the head and tail points for the same values of ζ as above. In this case, the difference between the time-histories for different ζ is significant even at the head point. This is due to the fact that the elastic waves in the shell propagate at a velocity that significantly exceeds the acoustic speed in the fluids. Thus, the head point 'feels' the elastic response caused by the internal wave reflection off the tail region much sooner, and this is why the plots start to differ significantly after $t \approx 1.8$. The same is even more true for the tail point where the dynamic responses are similar until about $t = 1.30$ (the time of arrival of the internal wave at the tail point for $\zeta = 1.50$), after which they differ considerably and are determined by the wave effects in the internal fluid.

10. Conclusions

A fully linear boundary-value problem was formulated for the interaction between a single submerged fluid-filled cylindrical shell and an external shock wave for the most general scenario where the internal and external fluids are different. A two-dimensional linear simplification of the problem was considered, and a semi-analytical solution was obtained.

Before summarizing our findings, we emphasize that because the model used here has been extensively validated in the author's earlier work [2,3] with the very good agreement with a number of experiments observed, the fact that no experimental data seem to exist for the interaction scenarios addressed here does not appear to be a limiting factor, and we believe it to be possible to state with some degree of confidence that the results presented here can be viewed as a reasonably close approximation of the reality.

The ratio of the internal and external acoustic speeds, ζ, was proposed as the single most important parameter determining the appearance of the acoustic fields induced by the interaction. Three distinctly different interaction scenarios were identified and analyzed: the scenario where the internal acoustic speed is lower than external, $\zeta < 1$ (termed the 'subsonic scenario'), the scenario where the internal and external fluids are identical, $\zeta = 1$ (the 'sonic scenario'), and the one where the internal acoustic speed is higher than external, $\zeta > 1$ (the 'supersonic scenario').

Even in the simplest case of $\zeta = 1$, a number of interesting effects were observed. Specifically, the Mach stems produced by the reflection of the pressure wave from the interior surface of the shell geometrically match the Mach stems of the external reflection, and the two sets of stems appear to be each other's geometrical continuation. This is a very interesting feature of the sonic interaction, and it adds, at another level, to the previously discussed notion of the transparency of a shell to an external shock wave. The multiple regular reflection that develops along the internal wall of the shell during the late interaction manifests itself in the external fluid as well, and it seems appropriate to refer to this phenomenon as 'leaking' of the multiple internal Mach stems into the external fluid. Thus, the influence of the effects in the internal fluid on the external field was emphasized, and it was reiterated that, from the acoustical analysis point of view, a fluid-filled shell is a much more active and phenomenologically complex source that its evacuated counterpart.

The supersonic scenario, $\zeta > 1$, resembles, in many respects, the sonic scenario, but all the phenomena occurring in the internal fluid are offset in time, and occur earlier than they would if the fluids were identical. The fundamental difference from the sonic case, however, is in the fact that due to the higher internal acoustic speed, the wave in the internal fluid propagates much faster than the scattered wave in the external one, and it radiates back into the external fluid in the regions that are not yet affected by the incident or scattered waves. As a result, one observes not one but *two* high-magnitude pressure fronts in the external fluid, one being the scattered wave, and the other the radiated wave in question, along with the low-magnitude shell-induced wave that propagates ahead of the two high-magnitude ones. The 'leaking' of the multiple Mach stems of the

internal reflection into the external fluid is observed as well, but the continuity between the primary Mach stems of the internal and external reflection is no longer the case.

The subsonic scenario, $\zeta<1$, is the most interesting of the three, and is also richest in terms of the diversity and complexity of wave reflection and focusing phenomena occurring. It is qualitatively different from the other two scenarios in what the internal pressure wave looks like and in the physics behind such appearance, and, depending on ζ, it can follow two different sub-scenarios. The first sub-scenario exhibits the familiar 'RF' sequence, with the peak focusing pressure only reached *after* the reflection. The second sub-scenario follows a very different, 'focusing–reflection–focusing' (FRF) sequence, with peak focusing pressure reached both *before* and *after* the reflection from the tail region takes place. The transition from the FRF to RF mode occurs at $\zeta \approx 0.52$, and when ζ is close to the transitional value, the first focusing occurs right on or very near the shell surface, thus coinciding with the reflection.

It is of particular practical importance that when ζ is significantly less than unity, the reflection and focusing sequences occur very late in the interaction, often at times when the incident wave not only has passed over the shell, but also moved away from it by its diameter or more. The existence of high pressure regions so late in the interaction certainly suggests redefining the time interval during which the maximum pressure is closely monitored, and prompts one to address the instants that would not be of any particular practical interest for the case of an evacuated shell, or even that of identical fluids inside and outside the shell. It is also interesting to point out that the front of the internal pressure wave in the subsonic case gradually changes its shape from concave to convex as ζ increases, and the transition between the two occurs at $\zeta \approx 0.86$ when the front is almost plane.

Another interesting and unique feature of the subsonic scenario is that when ζ is close enough to the critical value of 0.52, the reflection of the internal wave from the shell surface induces a distinct pressure wave in the external fluid and, effectively, one observes two different high-magnitude waves propagating downstream of the shell, the first being the scattered wave, and the second being the reflection-induced wave, the shape of its front closely resembling that of a shock wave with a source located at the tail point. A secondary but interesting feature of this external wave is that its front contacts the shell at the same points as the internal reflected wave that propagates upstream, which further supports the observations made earlier about the often present geometrical continuity existing between the internal and external wave reflection phenomena.

Several interesting ideas for future research stem out from this study. In particular, the observed diversity of wave reflection phenomena will, not doubt, have important implications when the stress-strain state of the shell is a primary concern, especially when a complete three-dimensional structural analysis is carried out. The possibility of cavitation in the system considered is of definite interest as well, even if the respective study will initially only be limited to hypothesizing about possible cavitation scenarios. The solution developed here is another addition to the series of converged analytical and semi-analytical solutions of shell-shock interaction problems that the author has been working on for some time, and it seems to be a suitable candidate for use as a benchmark for validating numerical codes.

Acknowledgments

The author gratefully acknowledges the financial support of the Natural Sciences and Engineering Research Council (NSERC) of Canada (Discovery Grant 261949), the Killam Trusts, and the Faculty of Engineering, Dalhousie University. The assistance of Garrett Dooley, a Mechanical Engineering student at Dalhousie University, is thankfully acknowledged as well. Mr. Dooley's participation in the project was possible through the NSERC Undergraduate Student Research Award (USRA) Program.

References

[1] R.D. Mindlin, H.H. Bleich, Response of an elastic cylindrical shell to a transverse step shock wave, *Journal of Applied Mechanics* 20 (1953) 189–195.

[2] J.H. Haywood, Response of an elastic cylindrical shell to a pressure pulse, *Quarterly Journal of Mechanics and Applied Mathematics* 11 (1958) 129–141.

[3] T.L. Geers, Excitation of an elastic cylindrical shell by a transient acoustic wave, *Journal of Applied Mechanics* 36 (1969) 459–469.

[4] T.L. Geers, Scattering of a transient acoustic wave by an elastic cylindrical shell, *Journal of the Acoustical Society of America* 51 (1972) 1640–1651.
[5] H. Huang, Y.F. Wang, Transient interaction of spherical acoustic waves and a cylindrical elastic shell, *Journal of the Acoustical Society of America* 48 (1970) 228–235.
[6] H. Huang, Scattering of spherical pressure pulses by a hard cylinder, *Journal of the Acoustical Society of America* 58 (1975) 310–317.
[7] A.E. Bryson, R.W.F. Gross, Diffraction of strong shocks by cones, cylinders, and spheres, *Journal of Fluid Mechanics* 10 (1961) 1–16.
[8] W.H. Heilig, Diffraction of a shock wave by a cylinder, *Physics of Fluids* 12 (Suppl. I) (1969) 154–157.
[9] W.G. Neubauer, L.R. Dragonette, Observation of waves radiated from circular cylinders caused by an incident pulse, *Journal of the Acoustical Society of America* 48 (1970) 1135–1149.
[10] W.G. Neubauer, Experimental observation of three types of pulsed circumferential waves on solid aluminium cylinders, *Journal of the Acoustical Society of America* 44 (1968) 1150–1152.
[11] W.G. Neubauer, Pulsed circumferential waves on aluminium cylinders in water, *Journal of the Acoustical Society of America* 45 (1968) 1134–1144.
[12] J.Y. Yang, Y. Liu, Computation of shock wave reflection by circular cylinders, *AIAA Journal* 25 (1987) 683–689.
[13] S. Eidelman, X. Yang, I. Lottati, Numerical simulation of shock wave reflection and diffraction in a dusty gas, *Proceedings of the 19th International Symposium on Shock Waves*, Marseille, France, July 1993, pp. 56–60.
[14] D.Kh. Ofengeim, D. Drikakis, Simulation of blast wave propagation over a cylinder, *Shock Waves* 7 (1997) 305–317.
[15] G. Heilig, Shock-induced flow past cylinders with various radii, *Proceedings of the 22nd International Symposium on Shock Waves*, Imperial College, London, UK, July 1999, pp. 1099–1104.
[16] J.G. Oakley, B.P. Puranik, M.H. Anderson, R.R. Peterson, R. Bonazza, R.P. Weaver, M.L. Gittings, An investigation of shock-cylinder interaction, *Proceedings of the 22nd International Symposium on Shock Waves*, Imperial College, London, UK, July 1999, pp. 941–946.
[17] Y. Takano, K. Hayashi, T. Goto, A computational procedure for interactions of shock waves with solid materials in liquid, *Proceedings of the 21st International Symposium on Shock Waves*, Great Keppel Island, Australia, July 1997, pp. 1039–1044.
[18] A. Merlen, P. Pernod, A. Ahyi, A. Kemmou, Shock-wave diffraction by an elastic sphere in water, *Proceedings of the 20th International Symposium on Shock Waves*, Vol. I, Pasadena, California, USA, July 1995, pp. 513–518.
[19] V. Latard, A. Merlen, V. Preobazhenski, A.C. Ahyi, Acoustic scattering of impulsive geometrical waves by a glass sphere in water, *Applied Physics Letters* 74 (1999) 1919–1921.
[20] U. Andelfinger, Simulations of underwater explosions against submerged structures using the DYSMAS/ELC code — Part A, *Proceedings of the 65th Shock and Vibration Symposium*, Vol. II, San Diego, California, USA, October 1994, pp. 243–251.
[21] A.C. Ahyi, P. Pernod, O. Gatti, V. Latard, A. Merlen, H. Uberall, Experimental demonstration of the pseudo-Rayleigh (A_0) wave, *Journal of the Acoustical Society of America* 104 (1999) 2727–2732.
[22] H. Sandusky, P. Chambers, F. Zerilli, L. Fabini, W. Gottwald, Dynamic measurements of plastic deformation in a water-filled aluminum tube in response to detonation of a small explosives charge, *Shock and Vibration* 6 (1999) 125–132.
[23] A.B. Wardlaw, J.A. Luton Jr, Fluid–structure interaction mechanisms for close-in explosions, *Shock and Vibration* 7 (2000) 265–275.
[24] G. Chambers, H. Sandusky, F. Zerilli, K. Rye, R. Tussing, J. Forbes, Pressure measurements on a deforming surface in response to an underwater explosion in a water-filled aluminum tube, *Shock and Vibration* 8 (2001) 1–7.
[25] H.U. Mair, Review: Hydrocodes for structural response to underwater explosions, *Shock and Vibration* 6 (1999) 81–96.
[26] H.U. Mair, Benchmarks for submerged structure response to underwater explosion, *Shock and Vibration* 6 (1999) 169–181.
[27] H. Huang, Transient response of two fluid-coupled spherical elastic shells to an incident pressure pulse, *Journal of the Acoustical Society of America* 65 (1979) 881–887.
[28] H. Huang, Transient response of two fluid-coupled cylindrical elastic shells to an incident pressure pulse, *Journal of Applied Mechanics* 46 (1979) 513–518.
[29] P. Zhang, T.L. Geers, Excitation of a fluid-filled, submerged spherical shell by a transient acoustic wave, *Journal of the Acoustical Society of America* 93 (1993) 696–705.
[30] M.A. Sprague, T.L. Geers, Response of empty and fluid-filled, submerged spherical shells to plane and spherical, step-exponential acoustic waves, *Shock and Vibration* 6 (1999) 147–157.
[31] S. Iakovlev, External shock loading on a submerged fluid-filled cylindrical shell, *Journal of Fluids and Structures* 22 (2006) 997–1028.
[32] S. Iakovlev, Submerged fluid-filled cylindrical shell subjected to a shock wave: Fluid-structure interaction effects, *Journal of Fluids and Structures* 23 (2007) 117–142.
[33] S. Iakovlev, Interaction between a submerged evacuated cylindrical shell and a shock wave. Part I: Diffraction-radiation analysis, *Journal of Fluids and Structures* 24 (2008) 1077–1097.
[34] S. Iakovlev, Interaction between a submerged evacuated cylindrical shell and a shock wave. Part II: Numerical aspects of the solution, *Journal of Fluids and Structures* 24 (2008) 1098–1119.
[35] M.C. Junger, D. Feit, *Sound, Structures and Their Interaction*, MIT Press, Cambridge, 1972.
[36] S. Iakovlev, Influence of a rigid co-axial core on the stress-strain state of a submerged fluid-filled circular cylindrical shell subjected to a shock wave, *Journal of Fluids and Structures* 19 (2004) 957–984.
[37] S. Iakovlev, Inverse Laplace transforms encountered in hyperbolic problems of non-stationary fluid-structure interaction, *Canadian Mathematical Bulletin* 50 (2007) 547–566.
[38] A. Selfridge, Approximate material properties in isotropic materails, *IEEE Transactions on Sonics and Ultrasonics* 32 (1985) 381–394.
[39] M. Sun, K. Takayama, A holographic interferometric study of shock wave focusing in a circular reflector, *Shock Waves* 6 (1996) 323–336.
[40] B.W. Skews, H. Kleine, Flow features resulting from shock wave impact on a cylindrical cavity, *Journal of Fluid Mechanics* 580 (2007) 481–493.